

# AN ALGORITHM FOR IDENTIFYING EIGENVECTORS EXHIBITING STRONG SPATIAL LOCALIZATION

JEFFREY S. OVALL AND ROBYN REID

ABSTRACT. We introduce an approach for exploring eigenvector localization phenomena for a class of (unbounded) selfadjoint operators. More specifically, given a target region and a tolerance, the algorithm identifies candidate eigenpairs for which the eigenvector is expected to be localized in the target region to within that tolerance. Theoretical results, together with detailed numerical illustrations of them, are provided that support our algorithm. A partial realization of the algorithm is described and tested, providing a proof of concept for the approach.

## 1. INTRODUCTION

This paper concerns the development of new computational methods for exploring eigenvector localization phenomena for selfadjoint elliptic eigenvalue problems,

$$(1) \quad \mathcal{L}\psi \doteq -\nabla \cdot (A\nabla\psi) + V\psi = \lambda\psi \text{ in } \Omega \quad , \quad \psi = 0 \text{ on } \partial\Omega \text{ , } \psi \not\equiv 0 \text{ in } \Omega \text{ ,}$$

where  $\Omega \subset \mathbb{R}^d$  is a bounded, connected open set,  $V \in L^\infty(\Omega)$  is non-negative, and there are constants  $c, C > 0$  such that the symmetric matrix  $A : \Omega \rightarrow \mathbb{R}^{d \times d}$  satisfies

$$c\mathbf{v}^t\mathbf{v} \leq \mathbf{v}^t A(x)\mathbf{v} \leq C\mathbf{v}^t\mathbf{v} \text{ for all } \mathbf{v} \in \mathbb{R}^d \text{ and a.e. } x \in \Omega \text{ .}$$

When  $d = 2$ , we require  $A \in [L^\infty(\Omega)]^{d \times d}$ ; and when  $d > 2$ , we require that  $A$  is uniformly Lipschitz in each of its components. The operator  $\mathcal{L}$  is viewed as an unbounded operator on  $L^2(\Omega)$ , with domain  $\text{Dom}(\mathcal{L}) = \{v \in H_0^1(\Omega) : \mathcal{L}v \in L^2(\Omega)\}$ . We denote the (real) spectrum of  $\mathcal{L}$  by  $\text{Spec}(\mathcal{L})$ , and recall that it consists of a sequence,  $\inf_\Omega V < \lambda_1 < \lambda_2 \leq \lambda_3 \leq \dots$ , that has no finite accumulation points. Furthermore, the eigenspace  $E(\lambda, \mathcal{L}) = \{v \in \text{Dom}(\mathcal{L}) : \mathcal{L}v = \lambda v\}$  is finite dimensional for each  $\lambda \in \text{Spec}(\mathcal{L})$ .

The assumptions on  $\mathcal{L}$  guarantee that it has the *unique continuation property* (cf. [1, 16, 23]), i.e. any function  $v \in H^1(\Omega)$  satisfying  $\mathcal{L}v = 0$  in  $\Omega$  that vanishes on a non-empty open subset of  $\Omega$  must vanish identically on  $\Omega$ . A simple consequence of this is that no eigenvector  $\psi$  of (1) may vanish identically on any open subset of  $\Omega$ . However, it may be the case that nearly all of the “mass” of an eigenfunction  $\psi$  is concentrated in a non-empty, open, proper subset  $R$  of  $\Omega$ . In this case, we say that  $\psi$  is *localized* in  $R$ . For convenience, we will refer to a non-empty, open, proper subset  $R$  of  $\Omega$  as a *subdomain* of  $\Omega$ . We now quantify what we mean by localization in  $R$ . Given a function  $v \in L^2(\Omega)$  and a subdomain  $R$ , the complementary quantities

$$(2) \quad \delta(v, R) = \|v\|_{L^2(\Omega \setminus R)} / \|v\|_{L^2(\Omega)} \quad , \quad \tau(v, R) = \|v\|_{L^2(R)} / \|v\|_{L^2(\Omega)} \quad ,$$

provide measures of localization/concentration of  $v$  within the subdomain  $R$ . Clearly,

$$\delta^2(v, R) + \tau^2(v, R) = 1 \quad , \quad \delta(v, R) = \tau(v, \Omega \setminus R) \quad , \quad \tau(v, R) = \delta(v, \Omega \setminus R) \quad ,$$

and we have  $\delta(\psi, R), \tau(\psi, R) \in (0, 1)$  for eigenvectors  $\psi$  and any subdomain  $R$ . Given a tolerance  $\delta^* \in (0, 1/2)$ , we say that  $v$  is *localized in  $R$  with tolerance  $\delta^*$*  if  $\delta(v, R) \leq \delta^*$  or, equivalently,  $\tau(v, R) \geq \sqrt{1 - (\delta^*)^2}$ . Note that we do not require that  $R$  is connected, although it will be in many applications.

Localization of eigenvectors may occur due to properties of the coefficients  $A$  and  $V$ , the shape of the domain, and/or the boundary conditions. A 2013 overview of the geometric structure of eigenvectors for  $\mathcal{L} = -\Delta$  that highlights eigenvector localization due to domain geometry is provided in [20] (see also [11, 22, 35, 38]). In a series of recent articles [4–6, 15], starting in 2012, the authors investigate localization due to highly discontinuous potentials  $V$  (“disordered media”), providing some theoretical insight into the mechanisms

driving localization, a novel numerical method for approximating likely subdomains in which localization may occur, and a simple estimate of the smallest eigenvalue whose eigenvector is localized in each such subdomain. In [15], the authors state that

“...there has been no general theory able to directly determine for any domain and any type of inhomogeneity the precise relationship between the geometry of the domain, the nature of the disorder, and the localization of vibrations, to predict in which subregions one can expect localized standing waves to appear, and in which frequency range.”

Although progress has been made by these authors and others (cf. [2, 3, 29, 34, 44]) in the meantime, there is still room for improvement, particularly on the algorithmic front. We describe the computational approaches of [4] and [2, 3], which are presented for Schrödinger operators  $\mathcal{L} = -\Delta + V$ , before giving a summary description of our own.

Central to the work in [4–6, 15] is the so-called *landscape function*  $u$  for  $\mathcal{L}$ . The following basic result, which is stated in each of these works, and can be proved by applying the Maximum Principle to  $w_{\pm} = \lambda\|\psi\|_{L^{\infty}(\Omega)}u \pm \psi$ , provides pointwise bounds on an eigenvector in terms of its eigenvalue and the landscape function.

**Proposition 1.1.** *Let  $(\lambda, \psi)$  be an eigenpair of (1). It holds that*

$$(3) \quad |\psi(x)| \leq \lambda u(x) \|\psi\|_{L^{\infty}(\Omega)}$$

*pointwise in  $\Omega$ , where  $u \in \text{Dom}(\mathcal{L})$ , satisfies  $\mathcal{L}u = 1$  in  $\Omega$ .*

An outline of the computational approach from [4] is:

- (a) Compute the landscape function  $u$ .
- (b) Determine several or all local minima of the associated *effective potential*  $W = 1/u$ ,  $W_k = W(x_k)$  for  $1 \leq k \leq N$ , with  $W_k \leq W_{k+1}$ .
- (c) Estimate  $N$  eigenvalues as  $\tilde{\lambda}_k = (1 + d/4)W_k$ . The factor  $(1 + d/4)$  is supported empirically and heuristically.
- (d) Choose the set  $R_k$  to be the connected component of  $\{x \in \Omega : W(x) \leq E\}$  that contains  $x_k$ , where  $E \geq \tilde{\lambda}_k$  is a parameter to be set by the user. It is expected that  $\delta(\psi, R_k)$  is small, where  $\psi$  is an eigenvector associated with the eigenvalue of  $\mathcal{L}$  estimated by  $\tilde{\lambda}_k$ .

We highlight a few features of this approach. The most obvious is that it does not involve the (approximate) solution of any eigenvalue problems; only the solution of a single source problem is required. From this, estimates (as opposed to convergent approximations) of several eigenvalues are computed, together with localization regions for eigenvectors whose eigenvalues are near the given estimates. *Eigenvector approximations are not provided*, though the authors mention solving for the smallest eigenpair of  $\mathcal{L}$  with homogeneous Dirichlet conditions on  $R_k$ , or some slightly larger region, as an option. We note that  $\tilde{\lambda}_k$ ,  $1 \leq k \leq N$ , are not necessarily estimates of the first  $N$  eigenvalues of  $\mathcal{L}$ . For example, there may be multiple eigenvectors that are localized in one or more of the regions  $R_1, \dots, R_k$  whose eigenvalues are smaller than the smallest eigenvalue having an eigenvector localized in  $R_{k+1}$ . We emphasize that the method of [4] estimates only the smallest eigenvalue having an eigenvector localized in a each of its determined subdomains  $R$ ; we will refer to this eigenvalue (or eigenpair) as the *ground state* for  $R$ .

In contrast, the approach of [2, 3], aims to compute localized eigenvectors (and their eigenvalues), together with their localization regions, by a two-phase iterative process. Given a highly disordered, but structured, potential  $V$ , a fine mesh  $\mathcal{T}^{\varepsilon}$  is generated that is deemed suitable for resolving the lowermost part of the spectrum of  $\mathcal{L}$  via a finite element method—the user determines the number  $N$  of eigenpairs sought. A (much) coarser mesh  $\mathcal{T}^H$ , of which  $\mathcal{T}^{\varepsilon}$  is a refinement, is used in the first phase of the algorithm, whose aim is to provide regions of localization, together with a basis for a rough approximation of the space in which approximate eigenpairs will be computed during the second phase. Starting with finite element hat functions associated with the vertices of  $\mathcal{T}^H$  (there should be at least  $3N$  of them), a few approximate inverse iterations, using one preconditioned conjugate gradient (PCG) step per iteration, are performed during phase one, with a mechanism involving Rayleigh quotients and a parameter  $\eta \in (0, 1)$  used pair down the set of functions after each iteration. At the end of phase one, a basis for a coarse subspace of dimension at least  $3N$  is obtained. Since  $\mathcal{T}^{\varepsilon}$  is a refinement of  $\mathcal{T}^H$  the functions obtained in phase one are already finite

element functions (of the same degree) on  $\mathcal{T}^\varepsilon$ . In phase two, a few steps of approximate inverse iteration are again used on the finer discretization, starting with the functions obtained from phase one; this time, however, three PCG steps are used per iteration. After each inverse iteration, approximate eigenpairs are obtained by a Rayleigh-Ritz procedure on the remaining set of functions, and a similar mechanism is used to pair down the set of functions (if needed) for the next iteration. At the end of phase two, a set of at least  $2N$  approximate eigenpairs is obtained, and the first  $N$  of them are kept. Variations on this basic algorithm are presented in [3], and the description above comes from Algorithm 1 in that paper. This algorithm is clearly more sophisticated and costly than that described above from [4], but it does provide approximations of eigenpairs, not just eigenvalues, and the quality of these approximations can be controlled by parameters in the discretization. Additionally, this algorithm can find more than one eigenvector that is localized in a given region, which was not the case for the approach of [4]. However, the authors note that their algorithm assumes that the first  $N$  eigenvectors are localized, which is a reasonable assumption for the highly disordered potentials they consider, but might be problematic for problems in which other factors, such as domain geometry, are dominant drivers of localization. The approach of [4] does not assume that the first  $N$  eigenfunctions are localized, but is currently limited to computing estimates of as many eigenvalues and localization subdomains as there are local minima of  $W = 1/u$ .

Both approaches discussed above are aimed at the lower part of the spectrum, and are best suited to situations in which this part of the spectrum contains many localized eigenvectors. Additionally, these approaches offer no a priori control of how strongly localized an eigenvector  $\psi$  should be in a localization subdomain  $R$  determined by their algorithms, i.e. how small  $\delta(\psi, R)$  should be, in order to consider it “localized enough”. Our approach puts this consideration at the forefront, and targets with the following fundamental task:

- (T) Given a subdomain  $R$ , an interval  $[a, b]$  and a (small) tolerance  $\delta^* > 0$ , find all eigenpairs  $(\lambda, \psi)$  for which  $\delta(\psi, R) \leq \delta^*$  and  $\lambda \in [a, b]$ , or determine that there are not any.

One might obtain reasonable candidates for such an  $R$  using a landscape function approach, as in [4], or the first phase of Algorithm 1 in [3], but for our purposes we will just assume an  $R$  is given. If  $[a, b]$  contains relatively few eigenvalues of  $\mathcal{L}$  (counted by multiplicity), this task can be accomplished reasonably efficiently using existing technology: just compute (approximate) all eigenpairs  $(\lambda, \psi)$  for  $\lambda \in [a, b]$  by your favorite method, and check  $\delta(\psi, R)$  for each. However, if  $[a, b]$  contains many eigenvalues of  $\mathcal{L}$ , or we have no a priori sense of how many eigenvalues it contains, an approach that automatically filters out eigenvectors that are not localized in  $R$  is desirable. Drawing inspiration from the work of Marletta [36, 37] on combating the effects of spectral pollution in computing eigenvalues for operators having essential spectrum, we also consider a complex-shifted version of the operator (though our operator  $\mathcal{L}$  has no essential spectrum). More specifically, given a subdomain  $R$  and a number  $s > 0$ , we define the normal operator  $\mathcal{L}_s$  by

$$(4) \quad \mathcal{L}_s = \mathcal{L} + is \chi_R \quad , \quad \text{Dom}(\mathcal{L}_s) = \text{Dom}(\mathcal{L}) \quad .$$

The intuition behind our approach is that, if  $(\lambda, \psi)$  is an eigenpair of  $\mathcal{L}$  with  $\psi$  highly localized in  $R$ , then there ought to be an eigenpair  $(\mu, \phi)$  of  $\mathcal{L}_s$  with  $\mu$  near  $\lambda + is$  and  $\phi$  near  $\psi$ . This intuition will be justified theoretically in Section 2. With this in mind, our algorithm template, Algorithm 1, begins by finding eigenpairs  $(\mu, \phi)$  of  $\mathcal{L}_s$  for which  $\Im \mu$  is near  $s$ . These eigenpairs of  $\mathcal{L}_s$  are then “post-processed” to find eigenpairs  $(\lambda, \psi)$  of  $\mathcal{L}$  for which  $\psi$  is likely to be localized in  $R$ . The parameter  $\delta^*$  governs both whether  $\Im(\mu)$  is “near enough” to  $s$ , and whether  $\delta(\psi, R)$  is “small enough”.

The rest of the paper is outlined as follows. In Section 2, we establish the key theoretical results that naturally lead to an algorithm template for (T), and illustrate several of the results and ideas of this section via two 1D examples for which discretization is not needed for computing eigenpairs of  $\mathcal{L}$  and  $\mathcal{L}_s$ . The algorithmic template itself is given in Section 3, together with a description of one reasonable choice for computing eigenpairs of  $\mathcal{L}_s$  that lie in a target region—the FEAST method. Section 4 contains several experiments illustrating the performance a practical realization of the algorithm using finite element discretizations to approximate eigenpairs. In Section 5 we offer a few concluding remarks.

## 2. THEORETICAL RESULTS AND ILLUSTRATIONS

Given a proper subdomain  $R$  and an  $s > 0$ , we now explain and justify what we mean by asserting that,

If  $(\lambda, \psi)$  is an eigenpair of  $\mathcal{L}$  with  $\psi$  highly localized in  $R$ , then there is an eigenpair  $(\mu, \phi)$  of  $\mathcal{L}_s$ , defined in (4), that is close to the eigenpair  $(\lambda + \mathbf{i}s, \psi)$  of  $\mathcal{L} + \mathbf{i}s$ .

A natural analogue of this assertion, with the roles of  $\mathcal{L}$  and  $\mathcal{L}_s$  reversed, also holds, and both will be considered below, after first establishing some simple bounds on the real and imaginary parts of eigenvalues of  $\mathcal{L}_s$ . Suppose that  $(\mu, \phi)$  is an eigenpair of  $\mathcal{L}_s$ . We have

$$(5) \quad \mu = \frac{(\mathcal{L}\phi, \phi)}{\|\phi\|_{L^2(\Omega)}^2} + \mathbf{i}s[\tau(\phi, R)]^2,$$

where  $(\cdot, \cdot)$  is the (complex) inner-product on  $L^2(\Omega)$ . It follows by the unique continuation principle and the variational characterization of the eigenvalues of  $\mathcal{L}$  that

**Proposition 2.1.** *For any  $\mu \in \text{Spec}(\mathcal{L}_s)$ ,  $0 < \Im\mu < s$  and  $\Re\mu > \lambda_1(\mathcal{L}) = \min \text{Spec}(\mathcal{L})$ .*

We now present the first of two key results concerning the eigenpairs of  $\mathcal{L}$ ,  $\mathcal{L}_s$  and  $\mathcal{L} + \mathbf{i}s$ .

**Theorem 2.2.** *Let  $(\lambda, \psi)$  be an eigenpair of  $\mathcal{L}$ . Then*

$$(6) \quad \text{dist}(\lambda + \mathbf{i}s, \text{Spec}(\mathcal{L}_s)) \leq s \delta(\psi, R).$$

Let  $\mu = \arg \min\{|\lambda + \mathbf{i}s - \sigma| : \sigma \in \text{Spec}(\mathcal{L}_s)\}$ . If  $M \subset \text{Spec}(\mathcal{L}_s)$  contains  $\mu$ , then

$$(7) \quad \inf_{v \in E(M, \mathcal{L}_s)} \frac{\|\psi - v\|_{L^2(\Omega)}}{\|\psi\|_{L^2(\Omega)}} \leq \frac{s \delta(\psi, R)}{\text{dist}(\lambda + \mathbf{i}s, \text{Spec}(\mathcal{L}_s) \setminus M)},$$

where  $E(M, \mathcal{L}_s) = \bigoplus\{E(\sigma, \mathcal{L}_s) : \sigma \in M\}$  is the invariant subspace for  $M$ .

*Proof.* Since  $\lambda + \mathbf{i}s \notin \text{Spec}(\mathcal{L}_s)$ ,  $(\lambda + \mathbf{i}s - \mathcal{L}_s)^{-1}$  is bounded and normal, and we have (cf. [30, Chapter 5, Section 3.5])

$$\|(\lambda + \mathbf{i}s - \mathcal{L}_s)^{-1}\|^{-1} = \text{dist}(\lambda + \mathbf{i}s, \text{Spec}(\mathcal{L}_s)).$$

We see by direct computation that  $(\lambda + \mathbf{i}s - \mathcal{L}_s)\psi = \mathbf{i}s \chi_{\Omega \setminus R} \psi$ , from which we obtain

$$\|\psi\|_{L^2(\Omega)} \leq \|(\lambda + \mathbf{i}s - \mathcal{L}_s)^{-1}\| s \|\psi\|_{L^2(\Omega \setminus R)}.$$

Rearranging terms, and using the definition of  $\delta(\psi, R)$ , completes the proof of (6).

Now let  $P_s = \frac{1}{2\pi\mathbf{i}} \int_\gamma (z - \mathcal{L}_s)^{-1} dz$  denote the (orthogonal) spectral projector for  $E(M, \mathcal{L}_s)$ . Here,  $\gamma \subset \mathbb{C}$  is any simple closed contour enclosing  $M$  and excluding  $\text{Spec}(\mathcal{L}_s) \setminus M$ . Noting that  $P_s$  commutes with  $\mathcal{L}_s$ , direct algebraic manipulation reveals that

$$(8) \quad I - P_s = (\lambda + \mathbf{i}s - \mathcal{L}_s(I - P_s))^{-1}(I - P_s)(\lambda + \mathbf{i}s - \mathcal{L}_s).$$

It follows that

$$(I - P_s)\psi = (\lambda + \mathbf{i}s - \mathcal{L}_s(I - P_s))^{-1}(I - P_s)\mathbf{i}s \chi_{\Omega \setminus R} \psi,$$

Therefore,

$$\|(I - P_s)\psi\|_{L^2(\Omega)} \leq \frac{s \|\psi\|_{L^2(\Omega \setminus R)}}{\text{dist}(\lambda + \mathbf{i}s, \text{Spec}(\mathcal{L}_s) \setminus M)},$$

which establishes (7). We note that it was not necessary that  $M$  contain  $\mu$  for (7) to hold, but that including  $\mu$  in  $M$  makes the demoninator larger. Of course, for (7) to be a meaningful bound, the term on the right must be less than 1, so including (at least)  $\mu$  in  $M$  is prudent.  $\square$

A simple consequence of Proposition 2.1 and Theorem 2.2, put in the context of our key task (T), is that

**Corollary 2.3.** *If  $(\lambda, \psi)$  is an eigenpair of  $\mathcal{L}$  with  $\lambda \in [a, b]$  and  $\delta(\psi, R) \leq \delta^*$ , then there is an eigenpair  $(\mu, \phi)$  of  $\mathcal{L}_s$  in the region  $U = U(a, b, s, \delta^*) = \{z \in \mathbb{C} : \text{dist}(z, L) \leq s\delta^*, \Im z < s\}$  pictured in Figure 1, where  $L = [a, b] + \mathbf{i}s$ .*

We also have the complementary result to Theorem 2.2, by similar reasoning.

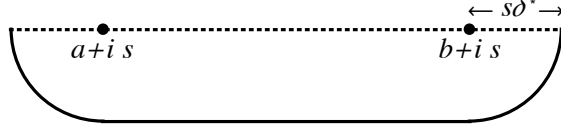


FIGURE 1. The region  $U = U(a, b, s, \delta^*)$  from Corollary 2.3.

**Theorem 2.4.** *Let  $(\mu, \phi)$  be an eigenpair of  $\mathcal{L}_s$ . Then*

$$(9) \quad s[\delta(\phi, R)]^2 \leq \text{dist}(\mu, \text{Spec}(\mathcal{L} + \mathbf{i}s)) \leq s\delta(\phi, R) ,$$

$$(10) \quad \text{dist}(\Re\mu, \text{Spec}(\mathcal{L})) \leq s\delta(\phi, R)\tau(\phi, R) .$$

Let  $\lambda = \arg \min\{|\sigma - \Re\mu| : \sigma \in \text{Spec}(\mathcal{L})\}$ . If  $\Lambda \subset \text{Spec}(\mathcal{L})$  contains  $\lambda$ , then

$$(11) \quad \inf_{v \in E(\Lambda, \mathcal{L})} \frac{\|\phi - v\|_{L^2(\Omega)}}{\|\phi\|_{L^2(\Omega)}} \leq \frac{s\delta(\phi, R)\tau(\phi, R)}{\text{dist}(\Re\mu, \text{Spec}(\mathcal{L}) \setminus (\Lambda \cup \{\Re\mu\}))} ,$$

where  $E(\Lambda, \mathcal{L})$  is the corresponding invariant subspace.

*Proof.* Since  $\mu \notin \text{Spec}(\mathcal{L} + \mathbf{i}s)$ , and  $(\mathcal{L} + \mathbf{i}s - \mu)\phi = \mathbf{i}s\chi_{\Omega \setminus R}\phi$ , the upper bound in (9) now follows in the same way as its counterpart (6). Since  $\mu = \mu_1 + \mathbf{i}s[\tau(\phi, R)]^2$ ,  $|d + \mathbf{i}s - \mu| = |d - \mu_1 + \mathbf{i}s[\delta(\phi, R)]^2| \geq s[\delta(\phi, R)]^2$  for any  $d \in \mathbb{R}$ , from which the lower bound follows immediately.

Letting  $\delta = \delta(\phi, R)$  and  $\tau = \tau(\phi, R)$ , one finds that  $(\mathcal{L} - \mu_1)\phi = \mathbf{i}s(\tau^2\chi_{\Omega \setminus R}\phi - \delta^2\chi_R\phi)$  by direct computation. If  $\mu_1 \in \text{Spec}(\mathcal{L})$ , then (10) holds trivially, so we assume that  $\mu_1 \notin \text{Spec}(\mathcal{L})$ . It follows that

$$\begin{aligned} \|\phi\|_{L^2(\Omega)}^2 &\leq \|(\mathcal{L} - \mu_1)^{-1}\|^2 \|\mathbf{i}s(\tau^2\chi_{\Omega \setminus R}\phi - \delta^2\chi_R\phi)\|_{L^2(\Omega)}^2 \\ &= \|(\mathcal{L} - \mu_1)^{-1}\|^2 s^2(\tau^4\|\phi\|_{L^2(\Omega \setminus R)}^2 + \delta^4\|\phi\|_{L^2(R)}^2) . \end{aligned}$$

Shifting around terms, and recalling that  $\delta^2 + \tau^2 = 1$ , we obtain gives

$$(12) \quad \|(\mathcal{L} - \mu_1)^{-1}\|^{-2} \leq s^2(\delta^4\tau^2 + \tau^4\delta^2) = s^2\delta^2\tau^2 ,$$

which yields (10).

Now let  $P = \frac{1}{2\pi\mathbf{i}} \int_{\gamma} (z - \mathcal{L})^{-1} dz$  denote the (orthogonal) spectral projector for  $E(\Lambda, \mathcal{L})$ , where  $\gamma$  is a simple closed contour that encloses  $\Lambda \cup \{\mu_1\}$ , and excludes  $\text{Spec}(\mathcal{L}) \setminus \Lambda$ . Noting that  $P$  commutes with  $\mathcal{L}$ , the identity

$$(13) \quad I - P = (\mathcal{L}(I - P) - \mu_1)^{-1}(I - P)(\mathcal{L} - \mu_1) ,$$

follows by direct algebraic manipulation. From this, (11) is achieved as before.  $\square$

*Remark 2.5* (Vector Normalization). Given an eigenpair  $(\mu, \phi)$  of  $\mathcal{L}_s$ , with  $\|\phi\|_{L^2(\Omega)} = 1$ , we will further normalize  $\phi$  as follows:

$$(14) \quad \phi \longleftarrow c\phi \text{ where } c = \arg \min\{\|\Im(d\phi)\|_{L^2(\Omega)} : |d| = 1\} .$$

Our rationale for minimizing the imaginary part in this sense is that if some scaling of  $\phi$ ,  $c\phi$ , is close to a real(!) eigenvector  $\psi$  of  $\mathcal{L}$ , which is the case if the upper-bound in (11) is small, then the imaginary part of  $c\phi$  should be small. Proposition 2.6 will provide further motivation for this kind of normalization. For a given non-zero function  $\phi = \phi_1 + \mathbf{i}\phi_2$ , not necessarily an eigenvector, one can recast the minimization problem  $\alpha = \min\{\|\Im(d\phi)\|_{L^2(\Omega)} : |d| = 1\}$  as a  $2 \times 2$  eigenvalue problem, with  $\alpha^2$  as the smaller of the two (real) eigenvalues. The corresponding real eigenvector  $\mathbf{c} = (c_1, c_2)$ , with  $c_1^2 + c_2^2 = 1$ , is related to the optimal scalar  $c$  by  $c = c_1 + \mathbf{i}c_2$ . The matrix for this eigenvalue problem is

$$(15) \quad \begin{pmatrix} \|\phi_2\|_{L^2(\Omega)}^2 & \int_{\Omega} \phi_1\phi_2 dx \\ \int_{\Omega} \phi_1\phi_2 dx & \|\phi_1\|_{L^2(\Omega)}^2 \end{pmatrix} .$$

It can be seen, using the Cauchy-Schwarz inequality, that this matrix is positive semidefinite, and that  $\alpha = 0$  iff  $\{\phi_1, \phi_2\}$  is a linearly dependent set.

**Proposition 2.6.** Let  $(\mu, \phi)$  be an eigenpair of  $\mathcal{L}_s$  with  $\|\phi\|_{L^2(\Omega)} = 1$ , and set  $\mu_1 = \Re\mu$ ,  $\phi_1 = \Re\phi$ ,  $\phi_2 = \Im\phi$ ,  $\tau = \tau(\phi, R)$  and  $\delta = \delta(\phi, R)$ . It holds that

$$(16) \quad \|(\mathcal{L} - \mu_1)\phi_1\|_{L^2(\Omega)}^2 = s^2(\tau^4\|\phi_2\|_{L^2(\Omega \setminus R)}^2 + \delta^4\|\phi_2\|_{L^2(R)}^2).$$

*Proof.* As was seen in the proof of Theorem 2.4,  $(\mathcal{L} - \mu_1)\phi = \mathbf{i}s(\tau^2\chi_{\Omega \setminus R}\phi - \delta^2\chi_R\phi)$ . Comparing the real and imaginary parts of both sides, we determine that

$$(\mathcal{L} - \mu_1)\phi_1 = -s(\tau^2\chi_{\Omega \setminus R}\phi_2 - \delta^2\chi_R\phi_2).$$

This identity immediately yields (16). □

The following 1D examples illustrate several of the ideas and results discussed so far.

*Example 2.7.* For  $\Omega = (0, 1)$ , we consider the operator

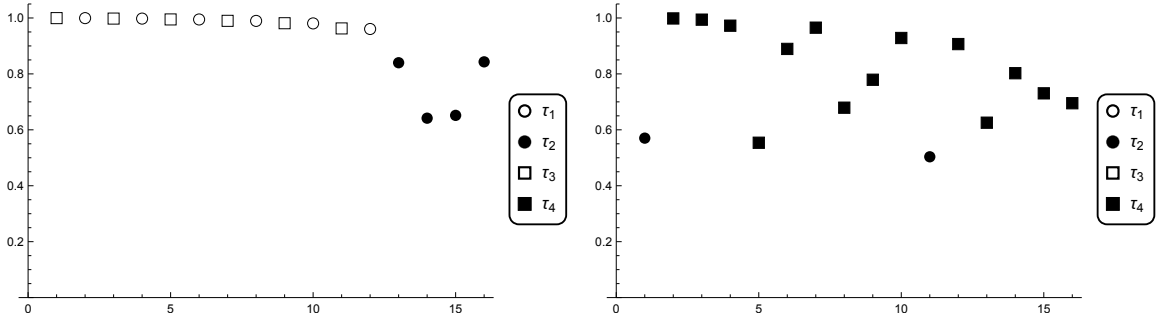
$$\mathcal{L} = -\frac{d^2}{dx^2} + \sum_{k=1}^4 V_k \chi_{R_k}, \quad R_k = \frac{1}{4}(k-1, k),$$

with homogeneous Dirichlet boundary conditions, for constants  $V_k \geq 0$ . The landscape function  $u$  can be determined analytically in this case. The eigenfunctions can also be determined analytically, up to the solutions of a non-linear equation for the eigenvalues (cf. [12]). As a concrete illustration, we consider the case  $(V_1, V_2, V_3, V_4) = (0, 80^2, 0, 400^2)$ . In this case,  $u$  has precisely two local maxima,  $u_1 = 0.008652$  and  $u_3 = 0.008819$ , at  $x_1 = 0.13155$  and  $x_3 = 0.61972$ , respectively. The approach of [4] estimates the two ground state eigenvalues as  $\lambda \approx 1.25/u_3 = 141.74280$  and  $\lambda \approx 1.25/u_1 = 144.46879$ ; the actual ground state eigenvalues in this case are  $\lambda = 140.49323$  and  $\lambda = 143.18099$ . Using the factor 1.875 employed in [4] for a (more complicated) 1D Schrödinger problem, the localization interval for the first ground state is  $[0.528993, 0.710441] \subset R_3$ , and for the second ground state, it is  $[0.0416835, 0.221412] \subset R_1$ .

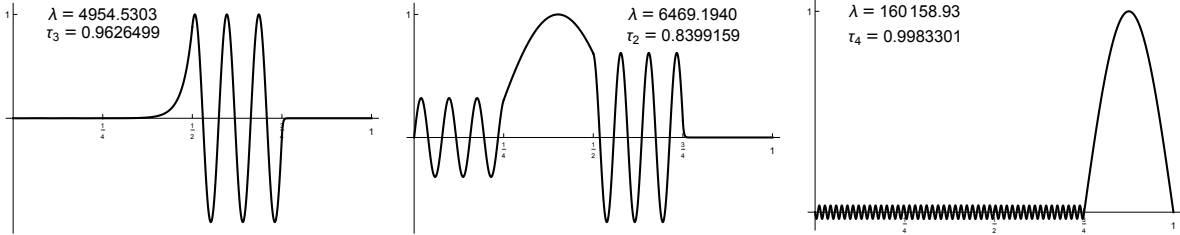
In Figure 2, plots are given of the maximum localization measures  $\max \tau_k = \max \tau(\psi, R_k)$ , for the eigenvectors associated with the smallest sixteen eigenvalues, and for the eigenvectors associated with first fifteen eigenvalues larger than  $V_4$  and the one immediately preceding them. The plot concerning eigenvalues near or larger than  $V_4$  was specifically chosen to demonstrate localization in the region  $R_4$ , which would not have been predicted in the approaches of [4] or [2, 3]. Plots of three eigenvectors are also given, together with their eigenvalues and the largest of their localization measures, to illustrate what “highly localized” may or may not look like in practice. With respect to the standard ordering of eigenvalues  $0 < \lambda_1 < \lambda_2 < \lambda_3 < \dots$  (all eigenvalues of  $\mathcal{L}$  are simple), the eigenpairs pictured in Figure 2(B) correspond to  $\lambda_{11}$ ,  $\lambda_{13}$  and  $\lambda_{96}$ . It is clear that  $\tau_k \leq 0.84$  does not correspond to a natural understanding of being highly localized in  $R_k$ , but that  $\tau_k \geq 0.96$  does, in these cases. The first twelve eigenvectors for this example, those for which  $\lambda < V_2 = 80^2$ , are all strongly localized in either  $R_1$  or  $R_3$ , alternating between these subdomains, with  $\max\{\tau_1, \tau_3\} > 0.96$ ; and the remaining four eigenvectors, though each most localized in  $R_2$ , are not highly localized in any of the four subdomains. Among the sixteen eigenvectors much higher in the spectrum, four of them are strongly localized in  $R_4$ , with  $\tau_4 > 0.96$ , the second, third, fourth and seventh; none of the rest are highly localized in any of the four subdomains.

A slight modification of the approach in [12] allows for the computation of complex eigenpairs for  $\mathcal{L}_s$ , and we use it below. In Table 1, we see the five eigenvalues  $\lambda$  of  $\mathcal{L}$  for which  $\lambda \in [0, 220000]$  and  $\delta(\psi, R_3) \leq \delta^* = 1/5$  for the corresponding eigenvector. The twelfth eigenvalue of  $\mathcal{L}$ ,  $\lambda = 4954.5303$ , just fails to make the cut, with  $\delta(\psi, R_3) = 0.27074936$ . For convenience in comparison, this eigenvalue and its localization measure are included in the table *in italics*. Also given in this table are all eigenvalues  $\mu$  of  $\mathcal{L}_s = \mathcal{L} + \mathbf{i}s\chi_{R_3}$  within the region  $U(0, 220000, s, \delta^*)$ , for  $s = 1$  and  $s = 100$ , together with the localization measures  $\delta(\phi, R_3)$  for their corresponding eigenvectors. In both cases for  $\mathcal{L}_s$ , six eigenpairs make the cut, with the final eigenvalue approximating  $\lambda = 4954.5303$ . Recalling (5), we note that  $\delta(\psi, R_3)$  can be obtained directly from  $\Im\mu$ ,  $\delta(\psi, R_3) = \sqrt{1 - \Im\mu/s}$ . When  $s = 1$ ,  $\lambda$  and  $\Re\mu$ , and  $\delta(\psi, R_3)$  and  $\delta(\phi, R_3)$ , agree in all digits shown, for eigenpairs  $(\lambda, \psi)$  and  $(\mu, \phi)$  that are matched. We note that there are 130 eigenvalues of  $\mathcal{L}$  in  $[0, 220000]$ , so the reduction to six candidates for localization in  $R$  is significant.

In Table 2, we see the two eigenvalues  $\lambda$  of  $\mathcal{L}$  for which  $\lambda \in [0, 220000]$  and  $\delta(\psi, R_4) \leq \delta^* = 1/5$  for the corresponding eigenvector. Also given in this table are all eigenvalues  $\mu$  of  $\mathcal{L}_s = \mathcal{L} + \mathbf{i}s\chi_{R_4}$  within the region  $U(0, 220000, s, \delta^*)$ , for  $s = 1$  and  $s = 100$ , together with the localization measures  $\delta(\phi, R_4)$  for their



(A)  $\max \tau_k$  for  $\lambda \in (140, 7155)$  (left) and  $\lambda \in (158923, 176357)$  (right)



(B) Three eigenvectors, with  $\lambda$  and  $\max \tau_k$ .

FIGURE 2. Localization measures  $\max \tau_k = \max \tau(\psi, R_k)$  for 32 eigenvectors, and plots of three of these eigenvectors, for Example 2.7.

corresponding eigenvectors. In both cases for  $\mathcal{L}_s$ , six eigenpairs make the cut, and the eigenvalues of  $\mathcal{L}$  that best match the remaining four of  $\mathcal{L}_s$ , together with their localization measures, are also given *in italics* in this table.

Finally, in Figure 3, analogues of the plots in Figure 2(B) are given for  $\mathcal{L}_s$ , with  $s = 100$ , and  $R = R_3$  for the first pair of plots,  $R = R_2$  for the second pair, and  $R = R_4$  for the third pair. Each pair of plots shows the real and imaginary parts of an eigenfunction  $\phi$ , normalized so that  $\|\phi\|_{L^2(\Omega)} = 1$  and  $\alpha = \|\Im \phi\|_{L^2(\Omega)}$  is minimized—see Remark 2.5. Up to scaling, the corresponding  $\psi$  and  $\phi_1 = \Re \phi$  show strong resemblances. Localization values  $\delta(\phi, R)$  and relative residuals  $\|(\mathcal{L} - \mu_1)\phi_1\|_{L^2(\Omega)} / \|\phi_1\|_{L^2(\Omega)}$  (see Proposition 2.6) are also included. The second eigenvector, shown in Figure 3(B), has the largest (worst)  $\delta$ -value,  $\alpha$ -value and relative residual among the three, whereas the third eigenvector is best in each of these categories. The  $\alpha$ -values in Table 1 for  $s = 100$  increased from  $7.189 \times 10^{-4}$  to  $5.337 \times 10^{-3}$  for the first five, and  $\alpha = 1.1015 \times 10^{-2}$  for the sixth. For the eigenvectors in Table 2 with  $s = 100$ ,  $\alpha = 4.152 \times 10^{-3}$  and  $\alpha = 8.870 \times 10^{-3}$  for the first two, and the  $\alpha$ -values ranged between  $1.515 \times 10^{-2}$  and  $2.613 \times 10^{-2}$  for the final four.

Based on the apparent correlation between a normalized eigenvector  $\phi$  of  $\mathcal{L}_s$  having a small  $\alpha$ -value and it being close to an eigenvector  $\psi$  of  $\mathcal{L}$  that is localized in  $R$ , one might be tempted think that  $\alpha$ -values for eigenvectors of  $\mathcal{L}_s$  are, *by themselves*, decent indicators of localization of eigenvectors of  $\mathcal{L}$  in  $R$ . However, this is not the case. For example, the second eigenvalue of  $\mathcal{L}_s$ , with  $s = 100$  and  $R = R_3$ , is  $\mu = 143.18098 + 6.2629546 \times 10^{-17}i$ , with the real part of the (normalized) eigenfunction  $\phi$  highly localized in  $R_1$ , and its significantly smaller imaginary part highly localized in  $R_3$ :  $\delta(\Re \phi, R_1) = 0.032815726$ ,  $\delta(\Im \phi, R_3) = 0.042859575$  and  $\alpha = 6.9038783 \times 10^{-10}$ . The eigenvector  $\phi$  of  $\mathcal{L}$  that is closest to  $\phi$  has  $\lambda = 143.18098$ ,  $\delta(\psi, R_1) = 0.032815726$  and  $\delta(\psi, R_3) = 1.0000000$ . So a small  $\alpha$ -value for  $\phi$  in this case corresponds to a nearby eigenvector of  $\mathcal{L}$  that is highly localized in the complement of  $R_3$ ! Of course, we never would have considered this eigenpair of  $\mathcal{L}_s$  if we were searching in the region  $U$  indicated in Corollary 2.3.

MATHEMATICA was used for all of these computations and plots, employing very high precision arithmetic.

*Example 2.8* (False Indication of Localization, Large  $s$ ). It can be the case that  $\mathcal{L}_s = \mathcal{L} + is\chi_R$  has localized eigenvectors even when  $\mathcal{L}$  has none. For example, if  $\mathcal{L} = -\frac{d^2}{dx^2}$  on  $(0, 1)$ , with homogeneous Dirichlet

TABLE 1. Eigenvalues and localization measures in  $R_3$  for eigenpairs  $(\lambda, \psi)$  of  $\mathcal{L}$  with  $\lambda \in [0, 220000]$  and  $\delta(\psi, R_3) \leq \delta^* = 1/5$ , for Example 2.7. Eigenvalues and localization measures for the eigenpairs  $(\mu, \phi)$  of  $\mathcal{L}_s$  with  $\mu \in U(0, 220000, s, 1/5)$ , for  $s = 1$  and  $s = 100$ . In italics are the eigenvalue and localization measure for  $\mathcal{L}$  that fail to satisfy  $\delta(\psi, R_3) \leq \delta^*$ , but which have obvious counterparts among the given eigenpairs of  $\mathcal{L}_s$ .

$\lambda$	$\delta(\psi, R_3)$	$s = 1$			$s = 100$		
		$\Re\mu$	$\Im\mu$	$\delta(\phi, R_3)$	$\Re\mu$	$\Im\mu$	$\delta(\phi, R_3)$
140.49323	0.0324770	140.49323	0.99894524	0.0324770	140.49441	99.894539	0.0324748
561.35749	0.0659934	561.35749	0.99564487	0.0659934	561.36244	99.564551	0.0659886
1260.5517	0.1019069	1260.5517	0.98961499	0.1019069	1260.5640	98.961665	0.1018987
2233.8447	0.1425062	2233.8447	0.97969199	0.1425062	2233.8708	97.969580	0.1424928
3472.5421	0.1928871	3472.5421	0.96279456	0.1928871	3472.5974	96.280425	0.1928620
<i>4954.5303</i>	<i>0.2707494</i>	4954.5303	0.92669479	0.2707494	4954.6877	92.674005	0.2706658

TABLE 2. Eigenvalues and localization measures in  $R_4$  for eigenpairs  $(\lambda, \psi)$  of  $\mathcal{L}$  with  $\lambda \in [0, 220000]$  and  $\delta(\psi, R_4) \leq \delta^* = 1/5$ , for Example 2.7. Eigenvalues and localization measures for the eigenpairs  $(\mu, \phi)$  of  $\mathcal{L}_s$  with  $\mu \in U(0, 220000, s, 1/5)$ , for  $s = 1$  and  $s = 100$ . In italics are the eigenvalues and localization measures for  $\mathcal{L}$  that fail to satisfy  $\delta(\psi, R_4) \leq \delta^*$ , but which have obvious counterparts among the given eigenpairs of  $\mathcal{L}_s$ .

$\lambda$	$\delta(\psi, R_4)$	$s = 1$			$s = 100$		
		$\Re\mu$	$\Im\mu$	$\delta(\phi, R_4)$	$\Re\mu$	$\Im\mu$	$\delta(\phi, R_4)$
160158.93	0.0577667	160158.93	0.99666301	0.0577667	160158.92	99.667632	0.0576513
160629.92	0.1092483	160629.92	0.98806481	0.1092483	160629.94	98.809982	0.1090879
<i>161389.73</i>	<i>0.2332336</i>	161389.73	0.94560213	0.2332335	161390.21	94.613050	0.2320981
<i>163942.68</i>	<i>0.2610104</i>	163942.68	0.93187361	0.2610103	163942.71	93.203093	0.2607088
<i>167673.57</i>	<i>0.3716197</i>	167673.57	0.86189881	0.3716197	167673.93	86.221341	0.3711962
<i>170192.99</i>	<i>0.4219290</i>	170192.99	0.82197599	0.4219289	170192.51	82.233071	0.4215084

conditions, the eigenpairs are  $(\lambda_n, \psi_n) = ((n\pi)^2, \sin(n\pi x))$ . Taking  $R = (0, 1/4)$ , we have

$$\frac{1}{4} \left(1 - \frac{2}{\pi}\right) \leq [\tau(\psi_n, R)]^2 = \frac{1}{4} \left(1 + \frac{i^{n+1} + (-i)^{n+1}}{n\pi}\right) \leq \frac{1}{4} \left(1 + \frac{2}{3\pi}\right), \quad [\tau(\psi_n, R)]^2 \rightarrow \frac{1}{4}.$$

Clearly, none of the eigenvectors are localized in  $R$ .

However, if we take  $s = 10^4$ , we find an eigenpair  $(\mu, \phi)$  of  $\mathcal{L}_s$  with  $\mu = 149.02494 + 9991.7736i$  and  $\delta(\phi, R) = 0.02868$ . In this case,  $\phi$  is highly localized in  $R$ , and  $\mu$  will lie in some  $U(a, b, s, \delta^*)$  for any  $\delta^* \geq 0.000822$ , which could lead to the false indicator that there is an eigenpair  $(\lambda, \psi)$  of  $\mathcal{L}$  with  $\psi$  highly localized in  $R$ . The nearest eigenvalue of  $\mathcal{L} + is$  to  $\mu$  is  $\lambda = (4\pi)^2 + is$ , with  $\psi = \psi_4$ , for which  $R$  is a nodal domain.

*Example 2.9* (False Indication of Localization, Small  $s$ ). One might wonder if only allowing smaller  $s$ , say  $s \approx 1$ , would eliminate such false indicators of localization of eigenvectors of  $\mathcal{L}$ , but that is not necessarily the case. Suppose that  $\mathcal{L} = -\frac{d^2}{dx^2} + V\chi_{(1/4, 3/4)}$ . It is straight-forward to show that eigenvectors of  $\mathcal{L}$  must have either even or odd symmetry about  $x = 1/2$ , so eigenvectors cannot be highly localized in either  $R = (0, 1/4)$  or  $R = (3/4, 1)$ . We also note that, being a Sturm-Liouville problem, the eigenvalues are known to be simple, but choosing large  $V$  can result in distinct eigenvalues that are very close. For our illustrations, we choose  $V = 80^2$ . The eigenvectors corresponding to the smallest two eigenvalues of  $\mathcal{L}$  are given in Figure 4. These eigenvalues are extremely close to each other,  $\lambda_2 - \lambda_1 \approx 3.59 \times 10^{-16}$ . Increasing  $V$  reduces this gap even further.

When  $R = (0, 1/4)$  and  $s = 1$  are chosen for  $\mathcal{L}_s$ , the eigenpair  $(\mu, \phi)$  having smallest real part  $\mu_1$  is given in Figure 4. For this eigenpair, we have  $\delta(\phi, R) = 0.032815726$ ,  $\|(\mathcal{L} - \mu_1)\phi_1\|_{L^2(\Omega)} / \|\phi_1\|_{L^2(\Omega)} = 7.27553 \times 10^{-6}$ , which is a very strong false(!) indicator of localization of an eigenvector  $\psi$  of  $\mathcal{L}$  having eigenvalue  $\lambda$  near  $\mu_1$ .



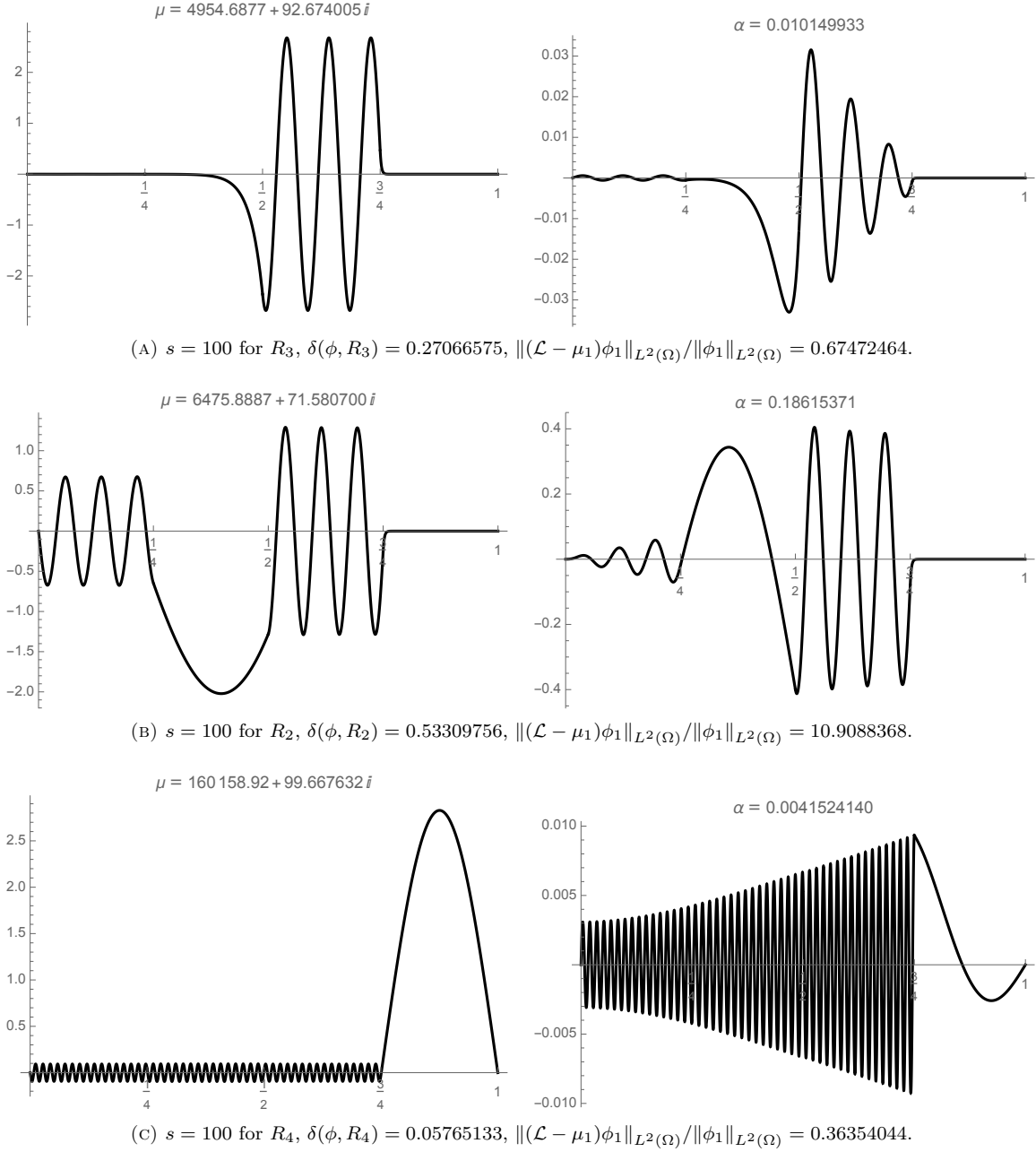


FIGURE 3. Plots of  $\phi_1 = \Re\phi$  (left) and  $\phi_2 = \Im\phi$  for eigenvectors  $\phi$  of  $\mathcal{L}_s$ , normalized so that  $\|\phi\|_{L^2(\Omega)} = 1$  and  $\alpha = \|\phi_2\|_{L^2(\Omega)}$  is minimized, for Example 2.7. The eigenvalues  $\mu = \mu_1 + i\mu_2$  are given above the plots of  $\phi_1$ , and the  $\alpha$ -values are given above the plots of  $\phi_2$ . Compare with Figure 2(B).

There is a counterpart of  $\lambda_2$  among the eigenvalues of  $\mathcal{L}_s$  as well, having real part  $143.180985607932844609$  (slightly larger than  $\mu_1 = \Re\mu$ ) and imaginary part  $3.2278925 \times 10^{-32}$ . The corresponding eigenvector is highly localized in  $(3/4, 1)$ . Motivated by this observation, we mention a simple analogue of (6) whose proof follows precisely the same pattern as that for (6) in Theorem 2.2. For an eigenpair  $(\lambda, \psi)$  of  $\mathcal{L}$ , it holds that

$$(17) \quad \text{dist}(\lambda, \text{Spec}(\mathcal{L}_s)) \leq s\tau(\psi, R) = s\delta(\psi, \Omega \setminus R) .$$

An obvious analogue for (7) holds as well, though we do not state it here.

Changing to  $R = (3/4, 1)$  yields essentially identical results as were obtained for  $R = (0, 1/4)$ , up to a flip in the graphs of the real and imaginary parts of  $\phi$  across  $x = 1/2$  and a change in signs. These are also given in Figure 4. If one had the inspired idea of taking  $R = (0, 1/4) \cup (3/4, 1)$ , the first two eigenpairs of  $\mathcal{L}_s$  (ordered by their real parts) are very close to those of  $\mathcal{L}$ . These are given in Figure 5.

Because of the tight clustering of eigenvalues of  $\mathcal{L}$ , we use this example to discuss the eigenvector result (11) in Theorem 2.4. With  $R = (0, 1/4)$ , the pair  $(\mu_1, \phi_1) = (\Re\mu, \Re\phi)$  associated corresponding to Figure 4 (B) has  $\mu_1$  very close to two eigenvalues of  $\mathcal{L}$ , those we called  $\lambda_1$  and  $\lambda_2$  above, but  $\phi_1$  is not close any eigenvector of  $\mathcal{L}$ . If we were to take  $\Lambda = \{\lambda_1\}$  or  $\Lambda = \{\lambda_2\}$  in (11), then the denominator in the bound,  $\text{dist}(\mu_1, \text{Spec}(\mathcal{L}) \setminus \Lambda)$ , is extremely small, which permits the poor approximation of  $\phi_1$  in  $E(\Lambda, \mathcal{L})$ . Note that  $\mu_1 \notin \text{Spec}(\mathcal{L})$ , so  $\text{Spec}(\mathcal{L}) \setminus (\Lambda \cup \{\mu_1\}) = \text{Spec}(\mathcal{L}) \setminus \Lambda$ , and so we use the more concise expression  $\text{dist}(\mu_1, \text{Spec}(\mathcal{L}) \setminus \Lambda)$ . However, if we take  $\Lambda = \{\lambda_1, \lambda_2\}$ , then  $\text{dist}(\mu_1, \text{Spec}(\mathcal{L}) \setminus \Lambda)$  is much larger, and a good approximation of  $\phi_1$  in  $E(\Lambda, \mathcal{L})$  is ensured. More specifically, the next closest eigenvalues of  $\mathcal{L}$  to  $\mu_1$  are  $\lambda_3 = 572.082899256658465449$  and  $\lambda_4 = 572.08289925665847099$ , so  $\text{dist}(\mu_1, \text{Spec}(\mathcal{L}) \setminus \Lambda) = \lambda_3 - \mu_1 = 428.90191$ . In this case, it is easy to see how  $\phi_1$  is very close to a linear combination of the eigenvectors of  $\mathcal{L}$  pictured in Figure 4(A); calling these  $\psi_1$  and  $\psi_2$ , we see that  $\phi_1 \approx -(\psi_1 + \psi_2)/\sqrt{2}$ .

As a matter of interest, we mention that the landscape function  $u$  for  $\mathcal{L}$  has a single local maximum value  $u_{\max} = 0.0086523880$ , which is achieved at  $x = x_{\max} = 0.13154762$  and  $x = 1 - x_{\max}$ . Using the approach of [4], the corresponding estimate of the smallest eigenvalue is  $\tilde{\lambda} = 1.25/u_{\max} = 144.46879$ . The summary description for finding a localization region  $R$  that was given in Section 1 is inadequate in this case, because both connected components of  $\{x \in \Omega : W(x) \geq E\}$  (for  $E \geq \tilde{\lambda}$ ) contain a minimizer of  $W = 1/u$ , and both components are of the same size, so such a consideration cannot be used as a tie-breaker. The authors of [4] note that tightly clustered minima and/or minimizers of  $W$  can make the choice of corresponding localization regions much more challenging, and indicate that they may pursue a more nuanced approach in the future.

*Remark 2.10.* As suggested by (17), one could easily develop results analogous to those in this section but for which the roles of  $R$  and  $\Omega \setminus R$  are “reversed”. While still being concerned with localization in  $R$ , the complex-shifted operator would be defined instead as  $\tilde{\mathcal{L}}_s = \mathcal{L} + i s \chi_{\Omega \setminus R}$ . The analogue of the statement given at the beginning of this section is:

If  $(\lambda, \psi)$  is an eigenpair of  $\mathcal{L}$  with  $\psi$  highly localized in  $R$ , then there will be an eigenpair  $(\mu, \phi)$  of  $\tilde{\mathcal{L}}_s$  that is close to  $(\lambda, \psi)$ .

The analogues of (6) and (10) in this case are

$$(18) \quad \text{dist}(\lambda, \text{Spec}(\tilde{\mathcal{L}}_s)) \leq s\delta(\psi, R) \quad , \quad \text{dist}(\Re\mu, \text{Spec}(\mathcal{L})) \leq s\delta(\phi, R)\tau(\phi, R) \quad ,$$

for eigenpairs  $(\lambda, \psi)$  of  $\mathcal{L}$  and  $(\mu, \phi)$  of  $\tilde{\mathcal{L}}_s$ . There are similarly predictable analogues of the other results in this section. A careful comparison of an approach based on  $\tilde{\mathcal{L}}_s$  with that based on  $\mathcal{L}_s$  is a topic of future research.

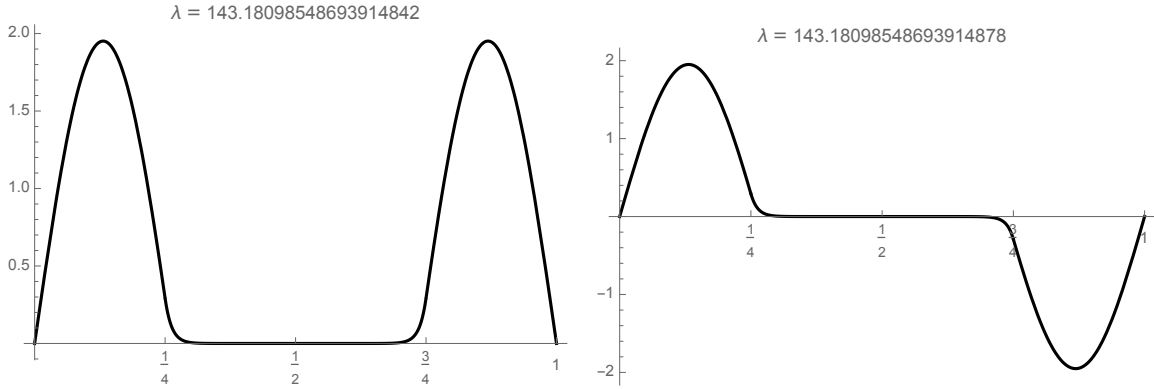
### 3. AN ALGORITHM TEMPLATE FOR (T)

Guided by the results of Section 2, we propose the algorithm template given in Algorithm 1 for our fundamental task (T), which we restate here for convenience,

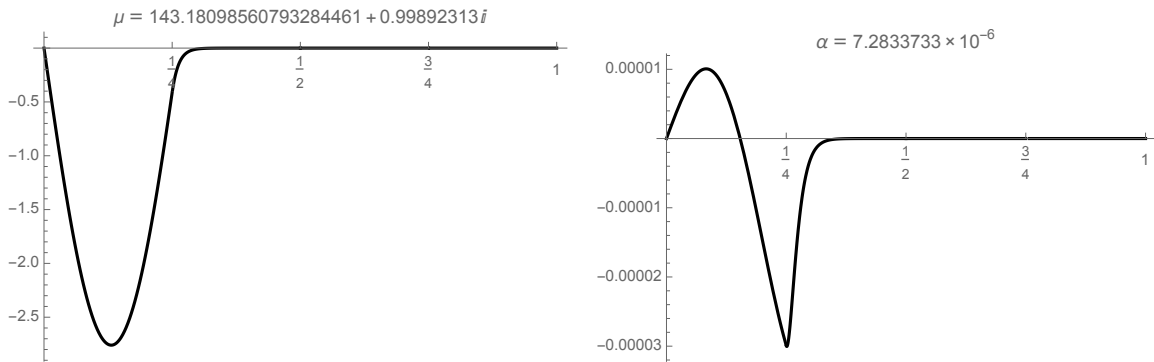
(T) Given a subdomain  $R$ , an interval  $[a, b]$  and a (small) tolerance  $\delta^* > 0$ , find all eigenpairs  $(\lambda, \psi)$  for which  $\delta(\psi, R) \leq \delta^*$  and  $\lambda \in [a, b]$ , or determine that there are not any.

Practical realizations are obtained by choices made on lines 2 and 8 of Algorithm 1, and we describe below reasonable choices for each. Tables 1 and 2, in which some eigenvalues of  $\mathcal{L}_s$  in  $U$  corresponded to an eigenvector of  $\mathcal{L}$  that was not sufficiently localized in  $R$ , demonstrate why line 9 is needed.

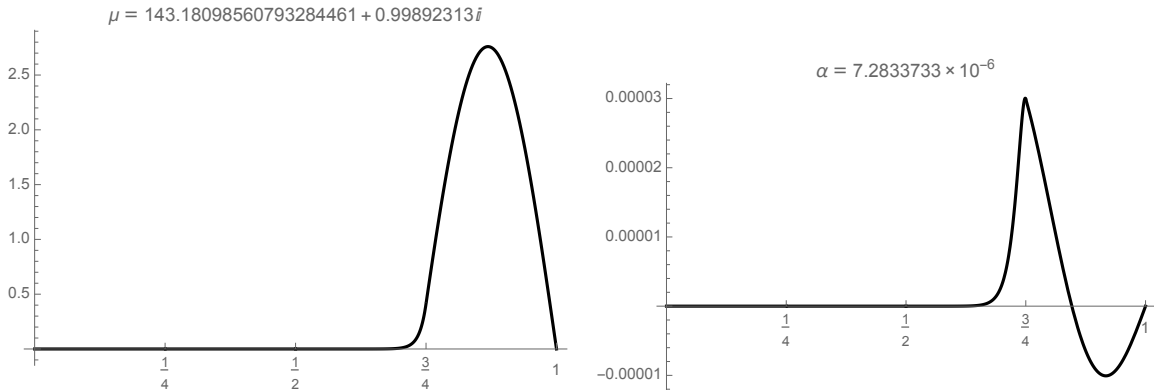
We first consider line 2 of Algorithm 1. There are several classes of methods that are designed for finding eigenpairs  $(\mu, \phi)$  (or just eigenvalues) of an operator, with  $\mu$  in some user-specified region  $\tilde{U} \subset \mathbb{C}$ , which we will assume is simply connected and has a (piecewise) smooth boundary  $\gamma = \partial\tilde{U}$ . We mention methods that are based on associated contour integrals, and classify them into four categories: Sakurai-Sugiura methods (SS, CIRR) (cf. [7, 27, 28, 40, 41, 52]), FEAST methods (cf. [17, 18, 24, 31, 39, 45, 49, 51]), Beyn methods



(A) The first two eigenvectors of  $\mathcal{L}$ .



(B) The real (left) and imaginary of the first eigenpair of  $\mathcal{L}_s$  with  $R = (0, 1/4)$ .

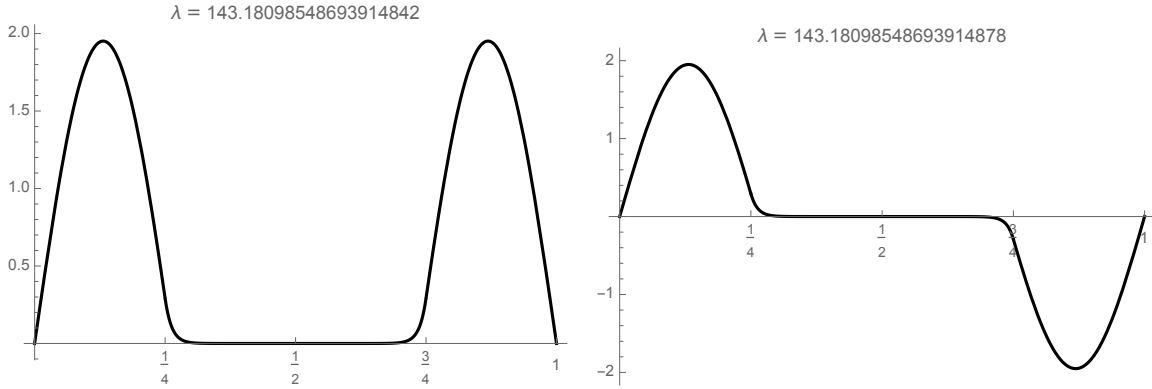


(C) The real (left) and imaginary of the first eigenpair of  $\mathcal{L}_s$  with  $R = (3/4, 1)$ .

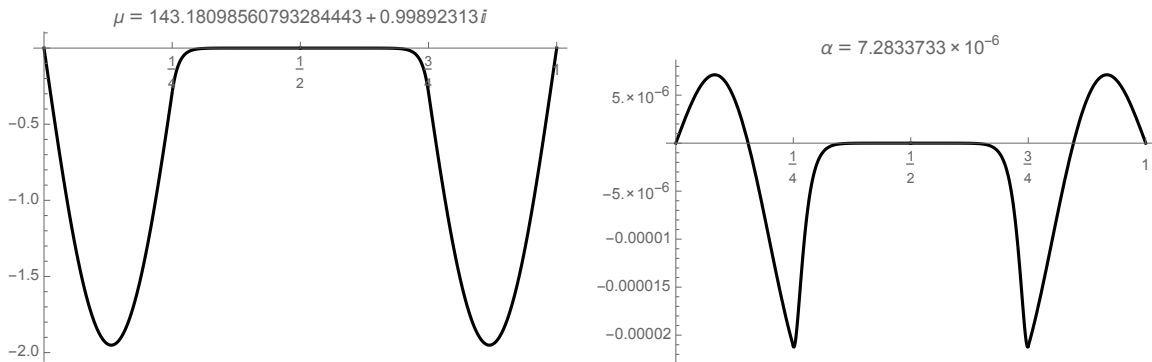
FIGURE 4. Plots of the first two eigenvectors of  $\mathcal{L}$ , and of the real and imaginary parts of the first eigenvector of  $\mathcal{L}_s$  for different choices of  $R$ , and  $s = 1$ . See Example 2.9.

(cf. [8–10, 32, 47]), and Spectral Indicator Methods (RIM, SIM) (cf. [25, 26, 33, 48]). Unlike the other three approaches, Spectral Indicators Methods do not involve the approximate solution of eigenvalue problems, and yield only eigenvalue approximations.

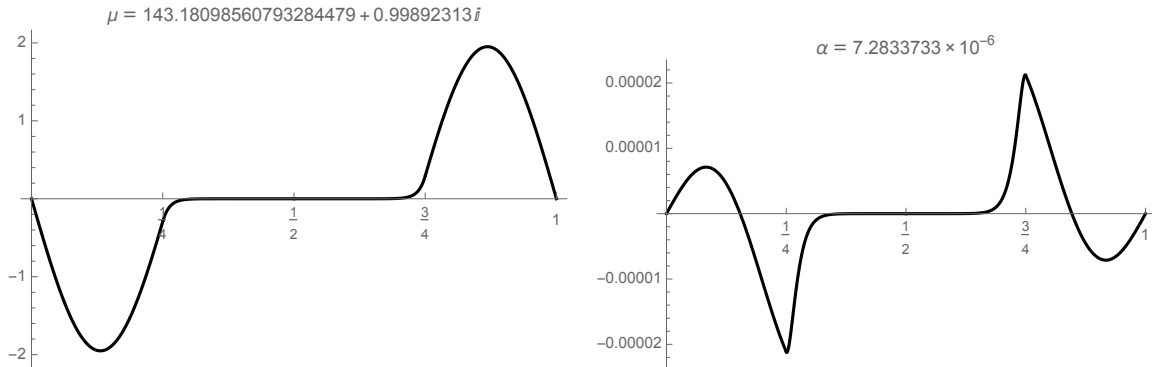
As we use the FEAST approach for our experiments in Section 4, we provide a brief high-level description of how it works for a normal (or selfadjoint) operator  $\mathcal{A}$  having compact resolvent, such as  $\mathcal{L}_s$  or  $\mathcal{L}$ . Although we are primarily concerned with applying FEAST to the normal operator  $\mathcal{L}_s$ , we describe it first for selfadjoint  $\mathcal{A}$ , and then indicate how it can be made applicable to normal operators. Suppose that  $f = f(z)$  is



(A) The first two eigenvectors of  $\mathcal{L}$ .



(B) The real (left) and imaginary of the first eigenpair of  $\mathcal{L}_s$  with  $R = (0, 1/4) \cup (3/4, 1)$ .



(C) The real (left) and imaginary of the second eigenpair of  $\mathcal{L}_s$  with  $R = (0, 1/4) \cup (3/4, 1)$ .

FIGURE 5. Plots of the first two eigenvectors of  $\mathcal{L}$ , and of the real and imaginary parts of the first eigenvector of  $\mathcal{L}_s$  for different choices of  $R$ , and  $s = 1$ . See Example 2.9.

a rational function that is bounded on  $\text{Spec}(\mathcal{A})$ . Then  $\mathcal{B} \doteq f(\mathcal{A})$  is a bounded (normal) operator on  $\text{Dom}(\mathcal{B}) \doteq \text{Dom}(\mathcal{A})$ , and if  $(\lambda, \psi)$  is an eigenpair of  $\mathcal{A}$ , then  $(f(\lambda), \psi)$  is an eigenpair of  $\mathcal{B}$ . We emphasize that the eigenvectors of  $\mathcal{A}$  and  $\mathcal{B}$  are the same! Now suppose that the open set  $\tilde{U}$  contains some finite subset  $\Lambda \subset \text{Spec}(\mathcal{A})$  and that the contour  $\gamma = \partial\tilde{U}$  does not intersect  $\text{Spec}(\mathcal{A})$ . The rational function  $f$  is then chosen as an approximation of the characteristic function for  $\tilde{U}$ ,  $f(z) \approx \chi_{\tilde{U}}(z) = \frac{1}{2\pi i} \oint_{\gamma} (\xi - z)^{-1} d\xi$ . This rational approximation is often obtained from a quadrature approximation of this Cauchy integral, taking the form  $f(z) = \sum_{k=0}^{n-1} w_k (z_k - z)^{-1}$ , but there are other ways of obtaining such a rational function

---

**Algorithm 1** Eigenvector Localization Template
 

---

```

1: procedure LOCALIZE( $a, b, s, \delta^*, R$ )
2:   determine all eigenpairs  $(\mu, \phi)$  of  $\mathcal{L}_s$  with  $\mu \in U(a, b, s, \delta^*)$  ▷ Corollary 2.3
3:   if no eigenvalues are found in 2 then
4:     exit ▷ There are no eigenpairs  $(\lambda, \psi)$  of  $\mathcal{L}$  with  $\lambda \in [a, b]$  and  $\delta(\psi, R) \leq \delta^*$ 
5:   else
6:     for each eigenpair  $(\mu, \phi)$  found in 2 do
7:        $\phi \leftarrow c\phi$  ▷ Normalize  $\phi$ , Remark 2.5
8:       post-process  $(\Re\mu, \Re\phi)$  to obtain (approximate) eigenpair  $(\tilde{\lambda}, \tilde{\psi})$  of  $\mathcal{L}$ 
9:       if  $\delta(\tilde{\psi}, R) \leq \delta^*$  then
10:        accept  $(\tilde{\lambda}, \tilde{\psi})$ 
11:       end if
12:     end for
13:   end if
14:   return accepted (approximate) eigenpairs  $(\tilde{\lambda}, \tilde{\psi})$ 
15: end procedure

```

---

(cf. [21, 46]). It follows that  $\mathcal{B}$  approximates (in some sense) the spectral projector  $S$  for  $\mathcal{A}$  associated with  $\Lambda$ , i.e.  $S = \chi_{\tilde{U}}(\mathcal{A}) = \frac{1}{2\pi i} \oint_{\gamma} (\xi - \mathcal{A})^{-1} d\xi$ . We have  $E \doteq \text{Range}(S) = E(\Lambda, \mathcal{A})$ , which is the target invariant subspace. FEAST is based on subspace iteration using the “filtered operator”  $\mathcal{B}$ : starting with a random finite-dimensional subspace  $E_0 \subset \text{Dom}(\mathcal{A})$  that satisfies  $SE_0 = E$ , the iteration generates a sequence of subspaces  $E_{k+1} = \mathcal{B}E_k$  that converge to  $E$  with respect to subspace gap. A Rayleigh-Ritz procedure is used on a finite rank operator  $\mathcal{A}_k : E_k \rightarrow E_k$  to obtain approximations  $\Lambda_k$  that converge to  $\Lambda$  in the Hausdorff metric, and a natural by-product of this procedure is that an orthonormal basis of  $E_k$  is obtained. More specifically,  $\mathcal{A}_k = P_k \mathcal{A}|_{E_k}$ , where  $P_k$  is the orthogonal projector onto  $E_k$ , and  $\Lambda_k = \text{Spec}(\mathcal{A}_k)$ . The rate of convergence is governed by the ratio

$$(19) \quad \kappa \doteq \frac{\sup_{\lambda \in \text{Spec}(\mathcal{A}) \setminus \Lambda} |f(z)|}{\inf_{\lambda \in \Lambda} |f(z)|} < 1 ,$$

so a good “filter function”  $f$  for the region  $\tilde{U}$  should decay rapidly (in modulus) away from  $\tilde{U}$ , and ideally not vary too much within  $\tilde{U}$ . For non-selfadjoint (normal)  $\mathcal{A}$ , approximations  $E_k$  and  $E_k^*$  of the right and left invariant subspaces  $E$  and  $E^*$  of  $\mathcal{A}$  are obtained using subspace iteration with  $\mathcal{B}$  and its adjoint  $\mathcal{B}^*$ , with some variations on how to extract eigenvalue approximations and maintain well-conditioned bases of  $E_k$  and  $E_k^*$  (cf. [31, 51]).

It is convenient to use

$$(20) \quad \tilde{U} = \tilde{U}(a, b, s, \delta^*) = \{z \in \mathbb{C} : \text{dist}(z, L) \leq s\delta^*\} \quad , \quad L = [a, b] + \mathbf{i}s ,$$

for the search region. Recall that the eigenvalues of  $\mathcal{L}_s$  that are of interest are in its lower-half,  $U$ , which is pictured in Figure 1. The region  $\tilde{U}$ , when viewed as a domain in  $\mathbb{R}^2$ , is often called a *Bunimovich stadium* in the context of quantum billiards, where it serves as a popular example (cf. [11]). We will refer to  $\gamma = \partial\tilde{U}$  as a *Bunimovich curve*. A unit-speed parameterization of  $\gamma$  that traverses it counter-clockwise, starting at the point  $b + \mathbf{i}(s - r)$ , is given by  $z(t) = x(t) + \mathbf{i}y(t)$ , where

$$(21) \quad (x(t), y(t)) = \begin{cases} r(\sin(\frac{t}{r}), -\cos(\frac{t}{r})) + (b, s) & , 0 \leq t \leq t_1 \\ (b + t_1 - t, s + r) & , t_1 \leq t \leq t_2 \\ r(\sin(\frac{t+a-b}{r}), -\cos(\frac{t+a-b}{r})) + (a, s) & , t_2 \leq t \leq t_3 \\ (a - t_3 + t, s - r) & , t_3 \leq t \leq P \end{cases} ,$$

and

$$(22) \quad r = s\delta^* , t_1 = \pi r , t_2 = t_1 + b - a , t_3 = t_2 + \pi r , P = 2\pi r + 2(b - a) .$$

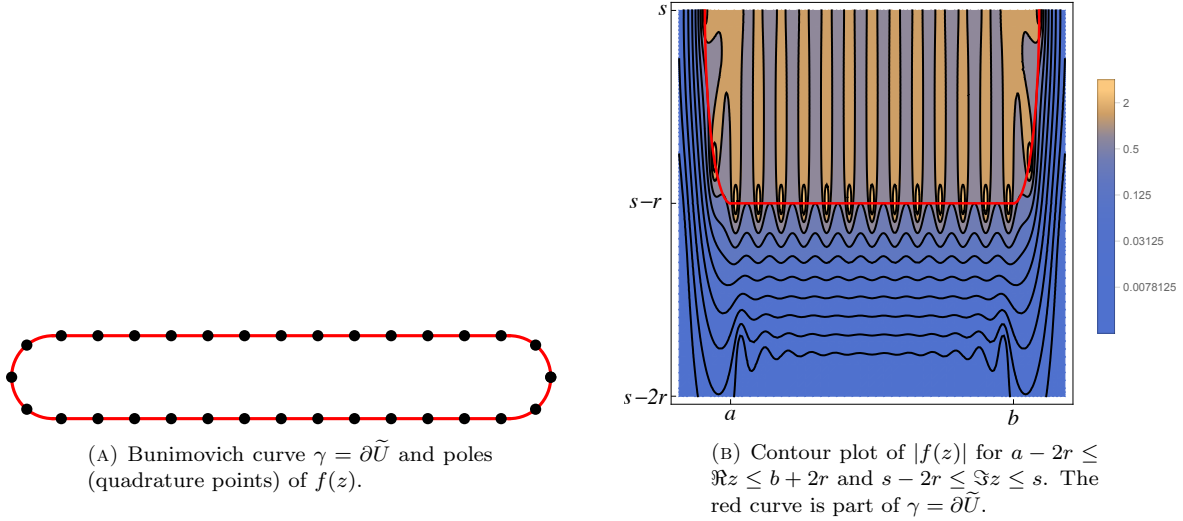


FIGURE 6. Poles and contour plot of  $|f(z)|$  for the rational filter  $f(z)$  associated with  $\tilde{U} = \tilde{U}(a, b, s, \delta^*)$  for  $(a, b, s, \delta^*) = (-4, 18, 10, 1/5)$ ;  $n = 32$  equispaced points are used for the filter.

The parameterization is made  $P$ -periodic by setting  $z(t + P) = z(t)$ . The  $n$ -pole rational filter function associated with  $\gamma$  is obtained by applying the trapezoid rule to  $\frac{1}{2\pi i} \oint_{\gamma} (\xi - z)^{-1} d\xi$ ,

$$(23) \quad f(z) = \sum_{k=0}^{n-1} w_k (z_k - z)^{-1} \quad , \quad z_k = z(kh + \pi r/2) \quad , \quad w_k = \frac{hz'(kh + \pi r/2)}{2\pi i} \quad , \quad h = \frac{P}{n} .$$

The offset of  $\pi r/2$  in the definition of the quadrature points (poles)  $z_k$  and weights  $w_k$  provides a more symmetric distribution of these points. An example Bunimovich curve, overlaid with the poles of  $f(z)$ , is given in Figure 6, together with a contour plot of  $|f(z)|$  that illustrates its effectiveness in distinguishing between points inside  $\gamma$  from those outside. The thick red curve in the contour plot is the portion of  $\gamma$  for which  $\Im z \leq s$ —recall that eigenvalues  $\mu$  of  $\mathcal{L}_s$  satisfy  $\Im \mu < s$ . The thick black curves in the contour plot are the contours  $|f(z)| = 2^j$ ,  $-8 \leq j \leq 2$ , with the curve for  $|f(z)| = 2^{-8}$  being farthest from  $\gamma$ . These indicate the desired rapid decay of  $|f(z)|$  away from  $\tilde{U}$ .

We now consider the post-processing step on line 8. As suggested by Theorem 2.4 and Proposition 2.6, the pair  $(\mu_1, \phi_1) = (\Re \mu, \Re \phi)$  is often a decent starting point for finding an eigenpair  $(\lambda, \psi)$  of  $\mathcal{L}$  with  $\lambda$  “close” to  $\mu_1$ ; recall that  $|\mu_1 - \lambda| \leq s\delta(\phi, R)\tau(\phi, R)$ . A reasonable post-processing procedure consists of a few inverse iterations, see Algorithm 2. One might instead opt for Rayleigh quotient iterations, which replace  $\mu_1$  with the

---

**Algorithm 2** Approximate Eigenpair Post-Processing

---

```

1: procedure POST-PROCESS( $\mu_1, \phi_1, \text{tol}$ )
2:    $\tilde{\lambda} \leftarrow \mu_1$ 
3:    $\tilde{\psi} \leftarrow \phi_1 / \|\phi_1\|_{L^2(\Omega)}$ 
4:   while  $\|\mathcal{L}\tilde{\psi} - \tilde{\lambda}\tilde{\psi}\|_{L^2(\Omega)} > \text{tol}$  do
5:      $\tilde{\psi} \leftarrow (\mu_1 - \mathcal{L})^{-1}\tilde{\psi}$ 
6:      $\tilde{\psi} \leftarrow \tilde{\psi} / \|\tilde{\psi}\|_{L^2(\Omega)}$ 
7:      $\tilde{\lambda} \leftarrow (\mathcal{L}\tilde{\psi}, \tilde{\psi})$ 
8:   end while
9:   return post-processed (approximate) eigenpair  $(\tilde{\lambda}, \tilde{\psi})$ 
10: end procedure

```

---

current approximation  $\tilde{\lambda}$  on line 5 of Algorithm 2. However, it is expected that few iterations will be needed, so requiring the action of only one inverse is perhaps more attractive. We note that Proposition 2.6 allows for the efficient computation of the initial residual, which may already be below the prescribed tolerance, resulting in no inverse iterations. In practice, one might use a more readily computable proxy for the residual norm.

In Remark 3.1 below, we highlight a potential danger of relying on the post-processing procedure in Algorithm 2 as stated in situations in which  $\mu_1 = \Re\mu$  is close to an eigenvalue of  $\mathcal{L}$ , but  $\phi_1 = \Re\phi$  is not close to an eigenvector despite the fact that  $\|\mathcal{L}\phi_1 - \mu_1\phi_1\|_{L^2(\Omega)}$  is reasonably small. Example 2.9 was chosen precisely to illustrate how such scenarios could arise. While we do not expect such situations to be common enough to reject Algorithm 2 as a viable option, it is useful to consider possible variants that are likely to be more robust in such situations. One such variant is to first estimate (as efficiently as possible) how many eigenvalues of  $\mathcal{L}$  are “near”  $\mu_1$  (cf. [14, 50]), as this has a direct affect on the convergence rate of inverse iteration. Recall that we are guaranteed that there is at least one eigenvalue of  $\mathcal{L}$  that is within  $s\delta(\phi, R)\tau(\phi, R)$  of  $\mu_1$ , so we might consider a slightly larger interval around  $\mu_1$  for our eigenvalue count estimate. If the approach estimates  $m$  eigenvalues of  $\mathcal{L}$  near  $\mu_1$ , then inverse iteration would be performed using a subspace of size at least  $m$ . After extracting (approximate) eigenpairs, each would be tested for its localization in  $R$ , as in lines 9-11 of Algorithm 1. A more in-depth discussion of variants of the post-processing algorithm will be postponed for subsequent work.

*Remark 3.1* (Possible False Positives from Post-Processing). As was demonstrated in Example 2.9, it is possible for  $\|\mathcal{L}\tilde{\psi} - \tilde{\lambda}\tilde{\psi}\|_{L^2(\Omega)}$  to be relatively small without  $(\tilde{\lambda}, \tilde{\psi})$  being close to an eigenpair of  $\mathcal{L}$ . In that example, we would have  $\|\mathcal{L}\tilde{\psi} - \tilde{\lambda}\tilde{\psi}\|_{L^2(\Omega)} = 7.27553 \times 10^{-6}$  for the initial check on line 4. If the tolerance in Algorithm 2 was chosen larger than this, no inverse iterations would be performed, and the procedure would return its input, which is not close to an eigenpair of  $\mathcal{L}$  and would falsely indicate an eigenvector of  $\mathcal{L}$  that is localized in  $R = (0, 1/4)$ . Setting a smaller tolerance in this case will force at least one inverse iteration, but the question of when the tolerance is small enough to be considered “safe” for the types of problems of interest is a subtle one. In fact, by increasing the constant  $V$  in Example 2.9, the initial residual  $\|\mathcal{L}\tilde{\psi} - \tilde{\lambda}\tilde{\psi}\|_{L^2(\Omega)}$  can be made arbitrarily small, so no tolerance would seem safe. For Example 2.9 with  $V = 80^2$  (as was used in that example), the form of  $(\mathcal{L} - \mu_1)^{-1}\tilde{\psi}$  is known in advance—linear combinations of (regular and/or hyperbolic) sines and cosines having known frequencies on each subinterval—so inverse iterations can be carried out by solving linear systems that enforce the boundary conditions and the continuity of the function and its derivative across subintervals. After performing the first inverse iteration, and renormalizing, the resulting function hardly differs from its predecessor at all—the maximal pointwise difference between the two functions is on the order of  $10^{-9}$ —which suggests that **many** inverse iterations would be required (in essentially exact arithmetic!) before the iterates began to reasonably approximate the true eigenvector. The extremely slow convergence of inverse iteration in this case is expected, due to the fact that there are two eigenvalues of  $\mathcal{L}$  that are extremely close to  $\mu_1$  (and to each other). Since the next nearest eigenvalues of  $\mathcal{L}$  are much farther away from  $\mu_1$ , performing inverse iteration with a two-dimensional subspace, (re)orthogonalizing its basis as needed, will lead to much more rapid convergence, from which (approximate) eigenpairs can be easily extracted using a Rayleigh-Ritz procedure. The initial basis might be chosen randomly, or one might choose  $\tilde{\psi} = \phi_1/\|\phi_1\|_{L^2(\Omega)}$  as one of the two basis functions and the other to be the normalized version of the orthogonal complement  $u^\perp$  of the landscape function  $u$  with respect to  $\phi_1$ , i.e.  $u^\perp = u - (u, \tilde{\psi})\tilde{\psi}$ . In this case, the “clever” choice of initial basis leads to very few inverse iterations before approximate eigenpairs very close to those given in Figure 4(A) are obtained by the Rayleigh-Ritz procedure. From these two, one can then deduce that there are no eigenvectors of  $\mathcal{L}$  whose eigenvalues are near  $\mu_1$  that are localized in  $R = (0, 1/4)$ , though one can see that they are localized in  $R = (0, 1/4) \cup (3/4, 1)$ .

*Remark 3.2.* As indicated near the beginning of this section, an approach such as SIM, which yields only eigenvalue approximations, might be used in line 2 of Algorithm 1. In this case, line 7 is clearly irrelevant, and the post-processing phase would proceed with only eigenvalue approximations. Since inverse iteration is used, and can proceed with random initialization, such an approach is feasible. The potential reduction in cost by using SIM on line 2 might make up for the potential increase in cost of using inverse iteration with *random* initialization, as opposed to the (likely) better initialization obtained from methods that return eigenpairs in line 2.

Up to this point, we have not discussed how to choose the parameter  $s$  in  $\mathcal{L}_s$ . Example 2.8 illustrates that choosing  $s$  “too large” can introduce false indicators of localization that would later have to be recognized and rejected, but how large is “too large” in terms of producing false indicators may be problem-dependent, as can be seen in Examples 2.7 and 2.9. In the first of these examples, choosing  $s = 1$  or  $s = 100$  had very little practical effect on the how well eigenpairs  $(\mu, \phi)$  of  $\mathcal{L}_s$  with  $\mu \in U(a, b, s, \delta^*)$  served as predictors of eigenpairs  $(\lambda, \phi)$  of  $\mathcal{L}$  for which  $\lambda \in [a, b]$  and  $\delta(\phi, R) \leq \delta^*$ . Example 2.9, which was specifically designed to yield false indicators of localization even when  $s$  is small, probably should not be weighed so heavily in coming up with practical guidance about how to choose  $s$ , but nonetheless illustrates that the quality of localization indicators coming from line 2 of Algorithm 1 can be quite sensitive to the choice of  $s$  for certain problems. Given the localization tolerance  $\delta^*$ , there is some theoretical appeal to choosing  $s$  so that  $r = s\delta^* \leq 1$ , because it makes it easier for the bounds in eigenvector results such as (7) and (11) to be meaningful (i.e. smaller than 1). However, Example 2.7 again shows that such a restriction is not necessary. It may be that a “good” choice of  $s$ , in relation to  $a, b$  and  $\delta$ , is dictated largely by practical efficiency considerations concerning the method used for computing eigenpairs  $(\mu, \phi)$  of  $\mathcal{L}_s$  with  $\mu \in U(a, b, s, \delta^*)$ . For example, with the FEAST approach used above, the rational filter  $f(z)$  determines how rapidly its iterations converge. We recall that the key issue is the contrast between  $|f(\mu)|$  for  $\mu \in U = U(a, b, s, \delta^*)$  and  $\mu \in \text{Spec}(\mathcal{L}_s) \setminus U$ ; the greater the contrast, the fewer number of iterations are needed. For fixed  $(a, b, s, \delta^*)$ , increasing the number  $n$  of poles in  $f$  (see (23)) will reduce the number of iterations needed, but increase the cost per iteration. For a fixed  $n$ , the aspect ratio of  $U$  (equivalently  $\tilde{U}$ ) affects the quality of the filter. In Figure 6,  $n = 32$  poles produces a very nice contrast for  $(a, b, s, \delta^*) = (-4, 18, 10, 1/5)$ ; the aspect ratio  $((b - a) + 2r)/(2r)$  is 6.5 in this case. However, changing only  $s$  from 10 to 1 increases the aspect ratio to 56, and destroys the quality of the filter. We do not picture the poor filter here, but mention that  $|f(z)| \geq 1/2$  for some  $z$  with  $\Im z = s - 2r$ ; the filter when  $s = 10$  satisfied  $|f(z)| < 2^{-7}$  (typically even smaller) for all such  $z$ . Now, taking  $(a, b, s, \delta^*) = (-4, -9/5, 1, 1/5)$  restores the aspect ratio of  $U$  to 6.5, and  $|f(z)|$  looks precisely as that pictured in Figure 6. We note that the only change between this and the “poor filter” situation is that  $b$  was changed to restore the original aspect ratio of 6.5. For a fixed  $U(a, b, s, \delta^*)$  (and  $n$ ), the situation can be improved by subdividing  $[a, b]$ ,  $[a, b] = [a_0, a_1] \cup \dots \cup [a_{p-1}, a_p]$  for some  $p \in \mathbb{N}$ , where  $a_j = a + j(b - a)/p$ . Each subregion  $U(a_j, a_{j+1}, s, \delta^*)$ , which will have a smaller aspect ratio than  $U(a, b, s, \delta^*)$ , can be searched independently (in parallel) for eigenvalues of  $\mathcal{L}_s$ . In light of the discussion above, it appears that offering practical guidance for choosing  $s$  may require significant experimentation, so we postpone such judgments to later work that is more computationally focused.

*Remark 3.3* (Alternate Approach Using Bounded Operator). As indicated above, when  $b - a$  is very large, the search region  $\tilde{U}(a, b, s, \delta^*)$  for eigenvalues of  $\mathcal{L}_s$  will typically have a very large aspect ratio, which would necessitate subdivision  $\tilde{U}(a, b, s, \delta^*) = \bigcup \{\tilde{U}(a_j, a_{j+1}, s, \delta^*) : 0 \leq j \leq p - 1\}$ . Since each subregion  $\tilde{U}(a_j, a_{j+1}, s, \delta^*)$  can be explored independently and in parallel, large regions can be efficiently explored in practice when parallel computing is available. However, a different approach might be used that requires only a single search region even if one wants to test all eigenvectors of  $\mathcal{L}$  for localization in  $R$ —assuming that there are only finitely many linearly independent eigenvectors of  $\mathcal{L}$  that are localized in  $R$  to within a given tolerance (see Remark 3.4 for a counterexample).

Suppose that  $\mathbf{b} > 0$  is a known or computed lower bound on  $\text{Spec}(\mathcal{L})$ . The eigenvectors of  $\mathcal{M} = \mathbf{b}\mathcal{L}^{-1}$  are precisely those of  $\mathcal{L}$ , and we have  $\text{Spec}(\mathcal{M}) \subset (0, 1]$ . If we define  $\mathcal{M}_s = \mathcal{M} + \mathbf{i} s \chi_R$ , then  $\text{Spec}(\mathcal{M}_s) \subset (0, 1] + \mathbf{i}(0, s)$ , and the obvious analogues of the results in Section 2 hold for  $\mathcal{M}$  and  $\mathcal{M}_s$ , as they did for  $\mathcal{L}$  and  $\mathcal{L}_s$ . Now, instead of exploring potentially many regions  $\tilde{U}(a_j, a_{j+1}, s, \delta^*)$  for eigenvalues of  $\mathcal{L}_s$ , we explore a single region  $\hat{U}(s, \delta^*) = [0, 1] + \mathbf{i}[s(1 - \delta^*), s]$  for eigenvalues of  $\mathcal{M}_s$ . Of course, this assumes that  $\hat{U}(s, \delta^*)$  contains only finitely many eigenvalues of  $\mathcal{M}_s$  counting multiplicities. The associated filtered operator  $\mathcal{B} = f(\mathcal{M}_s)$  for FEAST iterations has the form

$$(24) \quad \mathcal{B} = \sum_{k=0}^{n-1} w_k (z_k - \mathcal{M}_s)^{-1} = \mathcal{L} \sum_{k=0}^{n-1} w_k ((z_k - \mathbf{i} s \chi_R) \mathcal{L} - \mathbf{b})^{-1}.$$

A more thorough investigation of theoretical and practical considerations related to such an approach is intended for future work, though we note here that one must still contend with issues of discretization related to resolving highly oscillatory eigenvectors.



*Remark 3.4.* Although we expect that, when  $R$  is a relatively small subdomain of  $\Omega$ , and  $\delta^* < 1/2$ , there will typically be only finitely many eigenvectors  $\psi$  of  $\mathcal{L}$  that satisfy  $\delta(\psi, R) \leq \delta^*$ , this need not be the case. For example, let  $\Omega$  be the unit disk and  $\mathcal{L} = -\Delta$ . The eigenvalues are known to be  $\lambda_{m,n} = [j_n(m)]^2$ , for  $m \geq 1$  and  $n \geq 0$ , where  $j_\sigma(m)$  is the  $m$ th positive root of the first-kind Bessel function  $J_\sigma$ . The corresponding eigenspaces, expressed in polar coordinates, are

$$E(\lambda_{m,n}, \mathcal{L}) = \text{span}\{J_n(j_n(m)r) \sin(n\theta), J_n(j_n(m)r) \cos(n\theta)\} = \text{span}\{\psi_{m,n}^{(0)}, \psi_{m,n}^{(1)}\}.$$

Given  $r^* \in (0, 1)$ , we consider the annulus  $R$  for which  $r^* < r < 1$  ( $0 \leq \theta < 2\pi$ ). For  $n \geq 1$ , we have  $\|\psi_{m,n}^{(k)}\|_{L^2(\Omega)}^2 = (\pi/2)[J_{n+1}(j_n(m))]^2$ , and

$$[\delta(\psi_{m,n}^{(k)}, R)]^2 = \frac{(r^*)^2([J_n(j_n(m)r^*)]^2 - J_{n-1}(j_n(m)r^*)J_{n+1}(j_n(m)r^*))}{[J_{n+1}(j_n(m)r^*)]^2}.$$

It can be shown that  $\delta(\psi_{1,n}^{(k)}, R) \rightarrow 0$  as  $n \rightarrow \infty$ , regardless of the choice of  $r^*$ , which is a way of quantifying the statement that the eigenvectors  $\psi_{1,n}^{(k)}$  concentrate near the boundary of  $\Omega$  for large  $n$ . So we see that, even if  $r^*$  is near 1, so  $R$  is relatively small compared to  $\Omega$ , and  $\delta^*$  is small, there will be infinitely many linearly independent eigenvectors  $\psi$  of  $\mathcal{L}$  satisfying  $\delta(\psi, R) \leq \delta^*$ .

#### 4. A PARTIAL REALIZATION OF ALGORITHM 1

An implementation of the FEAST algorithm that uses finite element methods to discretize the associated operators is described in [17] (see also [18]). Corresponding code, Pythonic FEAST [19], builds on the general purpose finite element software package NGSolve [42, 43], and provides a convenient user interface in Python. Recent modifications to Pythonic FEAST allow for normal operators such as  $\mathcal{L}_s$ , which we use to illustrate a partial realization of Algorithm 1. In this realization, the computation (approximation) of eigenpairs of  $\mathcal{L}_s$  whose eigenvalues are in the search region  $U(a, b, s, \delta^*)$ , and the renormalization of the eigenvectors, is performed—up through line 7 of Algorithm 1. These computations provide likely candidates for associated localized eigenvectors of  $\mathcal{L}$ , to be obtained through post-processing and then finally accepted or rejected based on the tolerance  $\delta^*$ . The post-processing is not automated here, and we instead rely on visual comparison and experience to determine the eigenpairs of  $\mathcal{L}$  that correspond to those computed for  $\mathcal{L}_s$ . The final accept/reject decision for these eigenvectors of  $\mathcal{L}$  is clear based on their  $\delta$ -values.

To illustrate the implementation, we have chosen an example for which localization is due to domain geometry, as opposed to coefficients in the differential operator. The operator is  $\mathcal{L} = -\Delta$ , with homogeneous Dirichlet boundary conditions, and the domain  $\Omega$  consists of three squares, one  $4 \times 4$ , one  $3 \times 3$  and one  $2 \times 2$ , joined by two  $2 \times 1$  rectangular “bridges”, as shown in Figure 7. We refer to  $\Omega$  as the “three bulb” domain, and to each of the squares as “bulbs”. Many simple constructions such as this could be chosen to yield localization of some eigenvectors (cf. [13, 20]), and this domain was chosen because localization of eigenvectors in each of the three bulbs occurs (multiple times) early in the spectrum. The eigenvalue problems were discretized using quadratic finite elements on a fixed (relatively fine) quasi-uniform triangular mesh having maximal edge length 0.1, resulting a finite element space of dimension 15493.

To provide a baseline for comparison, we computed the first 71 eigenpairs for this discretization of  $\mathcal{L}$ , whose (discrete) eigenvalues are in the range (1.22, 33.30). Contour plots of the first sixteen eigenvectors are given in Figure 7, and exhibit instances localization in each of the three bulbs. In our localization experiments, we search for eigenvectors that are localized with tolerance  $\delta^* = 1/4$ , so  $\tau^* = \sqrt{15}/4 \approx 0.96825$ , in each of the three bulbs, for eigenvalues in [1, 33]. There are 70 such (discrete) eigenpairs in this portion of the spectrum. When  $R$  is taken to be the left bulb, 20 of these eigenvectors satisfy the localization tolerance. When  $R$  is taken as the right bulb, 9 of these eigenvectors satisfy the localization tolerance. Finally, when  $R$  is taken to be the middle bulb, only one of these eigenvectors satisfies the localization tolerance.

When  $R$  is taken as the middle bulb, two computed eigenpairs of  $\mathcal{L}_s$  are found having computed eigenvalues in  $U(1, 33, 1, \delta^*)$ . This search region was split into smaller (slightly overlapping) search regions as discussed in and before Remark 3.3, each having aspect ratio  $2/(2r) + 1 = 5$  ( $r = s\delta^* = 1/4$ ), that were tested independently using the Bunimovich filter having  $n = 32$  poles. These eigenvalues of  $\mathcal{L}_s$  were  $\mu = 4.50447 + 0.98218i$  and  $\mu = 24.33196 + 0.96185i$ . The corresponding eigenpairs of  $\mathcal{L}$  have  $\lambda = 4.50292$ , for which the eigenvector is sufficiently localized in  $R$ , and  $\lambda = 24.20972$ , for which its eigenvector  $\psi$  is not,  $\delta(\psi, R) =$

FIGURE 7. Contour plots of the first sixteen computed eigenvectors for the three bulb domain. Computed eigenvalues are given for each, as well as localization measures for the bulb in which the eigenvector is most localized:  $\tau_\ell$  for left bulb,  $\tau_r$  for right bulb, and  $\tau_m$  for middle bulb.

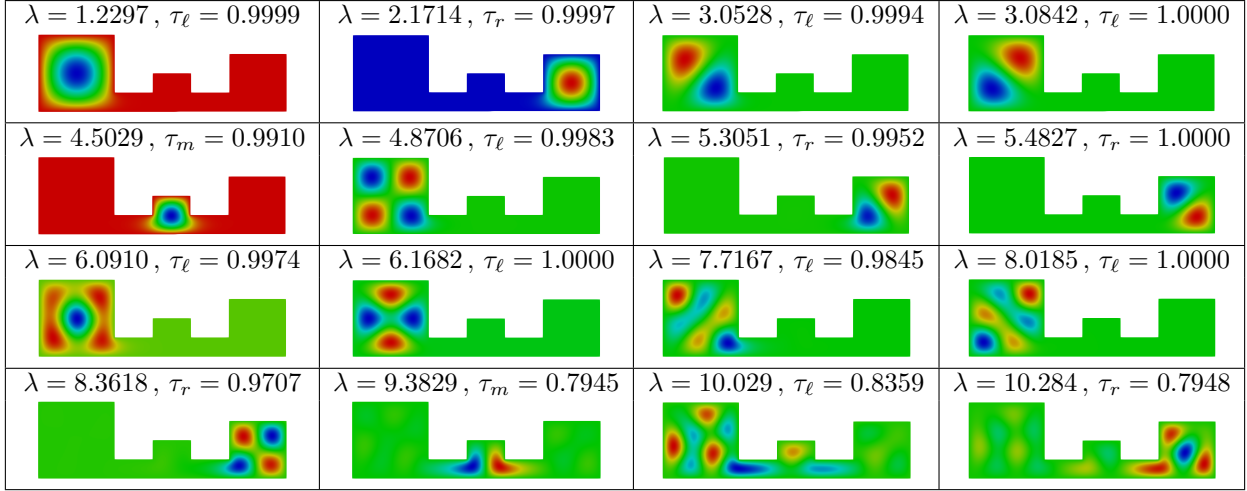
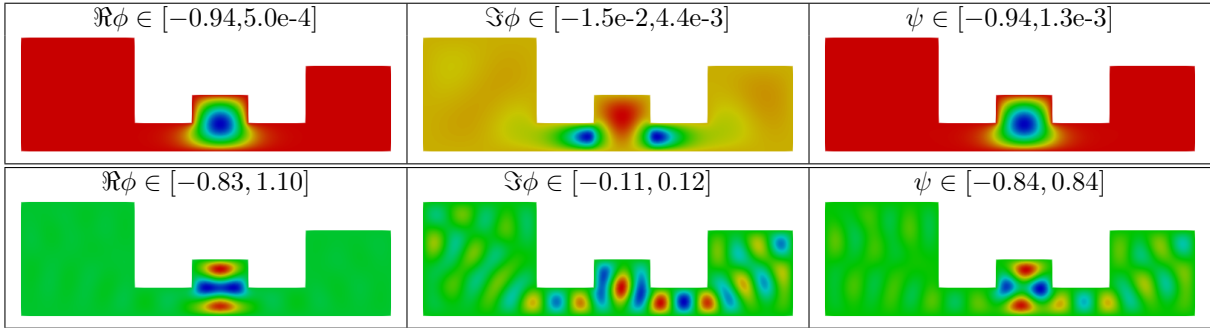


FIGURE 8. Middle bulb. Top panel: Contour plots of the eigenvector  $\phi$  of  $\mathcal{L}_s$  corresponding to the true indicator  $\mu = 4.50447 + 0.98218i$ , and of the matched eigenvector  $\psi$  of  $\mathcal{L}$  (with  $\lambda = 4.50292$ ). Bottom panel: Contour plots of the eigenvector  $\phi$  of  $\mathcal{L}_s$  corresponding to the false indicator  $\mu = 24.33196 + 0.96185i$ , and of the matched eigenvector  $\psi$  of  $\mathcal{L}$  (with  $\lambda = 24.20972$ ). The notation “ $f \in [c, d]$ ” in the images below indicates that the range of the function  $f$  shown in a given contour plot is  $[c, d]$ .



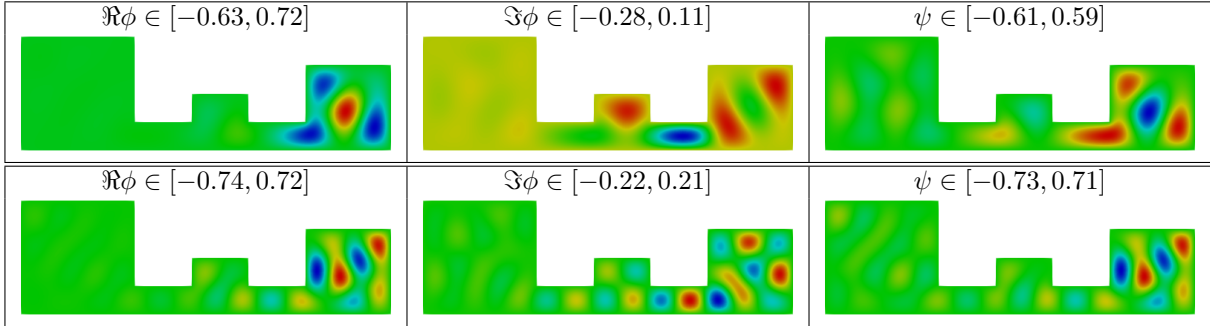
$0.64489 > \delta^*$  ( $\tau(\psi, R) = 0.76427 < \tau^*$ ). Contour plots of the real and imaginary parts of the eigenvectors  $\phi$  are given, together with their matched (real) eigenvectors  $\psi$ , in Figure 8. Since the color scheme in each image is relative to the range of values of the plotted function (blue for the smallest values and red for the largest), the ranges of function values are given explicitly in the figures for added context. We note that  $\max |\Im\phi|$  is significantly smaller than  $\max |\Re\phi|$  for the true indicator—about two orders of magnitude. For the false indicator, the difference is about one order of magnitude.

When  $R$  is taken as the right bulb, 14 computed eigenpairs of  $\mathcal{L}_s$  were found whose eigenvalues were in  $U(1, 33, 1, \delta^*)$ . This search was conducted in the same way for the middle bulb. Since there are only 9 eigenvectors of  $\mathcal{L}$  that are localized in  $R$  within the tolerance  $\delta^*$ , five of the eigenpairs of  $\mathcal{L}_s$  provide false indicators in this case. All 14 eigenvalues of  $\mathcal{L}_s$  are given in Table 3, together with the eigenvalues of  $\mathcal{L}$  with which we have matched them and the localization measures ( $\delta$ -values) of the corresponding eigenvectors of  $\mathcal{L}$ . Those that fail to make the final cut are emphasized using italics. Of the five false indicators, a strong case could be made that three of the corresponding eigenvectors  $\psi$  of  $\mathcal{L}$  just barely failed to make the cut—those

$\Re\mu$	$\Im\mu$	$\lambda$	$\delta(\psi, R)$	$\Re\mu$	$\Im\mu$	$\lambda$	$\delta(\psi, R)$
2.17146	0.99932	2.17143	0.02610	<i>18.61842</i>	<i>0.99841</i>	<i>18.62201</i>	<i>0.32601</i>
5.30605	0.99047	5.30506	0.09800	<i>18.98014</i>	<i>0.83889</i>	<i>18.98051</i>	<i>0.48562</i>
5.48270	1.00000	5.48270	0.00638	21.86147	0.99711	21.86307	0.07712
8.37589	0.94815	8.36148	0.24017	27.32128	0.99505	27.32821	0.18688
<i>10.41327</i>	<i>0.82496</i>	<i>10.28357</i>	<i>0.60658</i>	<i>28.12641</i>	<i>0.90667</i>	<i>28.15248</i>	<i>0.33336</i>
10.96057	0.99984	10.96061	0.02829	28.48136	0.99618	28.48221	0.06920
14.24624	0.99981	14.24624	0.01599	<i>31.58901</i>	<i>0.97649</i>	<i>31.58960</i>	<i>0.27542</i>

TABLE 3. Computed eigenvalues  $\mu$  of  $\mathcal{L}_s$  in  $U(1, 33, 1, \delta^*)$  for the right bulb, paired with matched eigenvalues  $\lambda$  of  $\mathcal{L}$  and localization measures  $\delta(\psi, R)$  of their corresponding eigenvectors  $\phi$ . The five false indicators are highlighted in italics.

FIGURE 9. Right bulb. Top panel: Contour plots of the eigenvector  $\phi$  of  $\mathcal{L}_s$  corresponding to the false indicator  $\mu = 10.41327 + 0.82496i$ , and of the matched eigenvector  $\psi$  of  $\mathcal{L}$  (with  $\lambda = 10.28357$ ). Bottom panel: Contour plots of the eigenvector  $\phi$  of  $\mathcal{L}_s$  corresponding to the false indicator  $\mu = 18.98014 + 0.83889i$ , and of the matched eigenvector  $\psi$  of  $\mathcal{L}$  (with  $\lambda = 18.98051$ ).



for which  $0.25 < \delta(\psi, R) < 0.34$ . In Figure 9 we provide contour plots, analogous to those in Figure 8, for the remaining two false indicators and their matched eigenvectors of  $\mathcal{L}$ .

We finally turn to the investigation of localization in the left bulb. For this choice of  $R$ , there are 20 eigenvectors of  $\mathcal{L}$  that satisfy the localization tolerance. Taking  $U(1, 33, 1, \delta^*)$  as before, we compute 29 eigenpairs of  $\mathcal{L}_s$ , so there are 9 false indicators in this case. Table 4, analogous to Table 3 for the right bulb, provides the corresponding numerical data. Of the 9 false indicators, only three (perhaps 4) really miss the mark in their predictions of localization for the matched eigenvectors of  $\mathcal{L}$ . We also performed the search with  $s = 1/2$ , for eigenpairs of  $\mathcal{L}_s$  with eigenvalues in  $U(1, 33, 1/2, \delta^*)$ . In lieu of the level of detail provided in Table 4, we summarize the results. The choice of  $s = 1/2$  yielded 28 candidates, with one fewer false indicator, corresponding to  $\lambda = 30.99216$ . Changing to  $s = 1/4$  eliminated two more false indicators, those corresponding to  $\lambda = 10.02874$  and  $\lambda = 10.84459$ . Further reducing to  $s = 1/8, 1/16, 1/32$  or  $1/64$  did not eliminate any of the remaining false indicators.

## 5. CONCLUDING REMARKS

We have provided theory, together with detailed examples illustrating key results, motivating Algorithm 1 for exploring eigenvector localization phenomena. A partial realization of Algorithm 1 was described and tested on a problem exhibiting multiple instances of localization due to domain geometry early in its spectrum, providing a “proof of concept” for our approach. What is missing from this realization is a post-processing phase in which eigenpairs of  $\mathcal{L}$  are obtained from those of  $\mathcal{L}_s$  automatically, though some form of inverse iteration was suggested for this. We have not provided *numerical analysis*, i.e. theoretical insight into the effects of discretization errors, for our approach, but intend to pursue that in future work. Future work will also include extensive testing of a full realization of Algorithm 1, as well as variants discussed

$\Re(\mu)$	$\Im(\mu)$	$\lambda$	$\delta(\psi, R)$	$\Re(\mu)$	$\Im(\mu)$	$\lambda$	$\delta(\psi, R)$
1.22976	0.99989	1.22975	0.01043	17.86628	0.99922	17.86930	0.03231
3.05287	0.99882	3.05277	0.03393	20.94272	0.99914	20.94341	0.06392
3.08423	1.00000	3.08423	0.00046	<i>22.62970</i>	<i>0.99581</i>	<i>22.58585</i>	<i>0.44630</i>
4.87100	0.99661	4.87063	0.05798	22.81320	0.99887	22.81332	0.03824
6.09172	0.99482	6.09100	0.07199	24.62085	0.99792	24.62379	0.13433
6.16815	1.00000	6.16815	0.00195	<i>24.87619</i>	<i>0.94232</i>	<i>24.89579</i>	<i>0.32321</i>
7.72286	0.97045	7.71673	0.17517	25.27439	0.88857	25.27430	0.02228
8.01849	0.99999	8.01849	0.00263	27.67153	0.99504	27.67714	0.14656
<i>10.14045</i>	<i>0.84445</i>	<i>10.02874</i>	<i>0.54897</i>	30.70848	0.99543	30.70761	0.07065
10.48456	0.99995	10.48453	0.01301	30.84404	0.99999	30.84395	0.00292
<i>10.77238</i>	<i>0.91878</i>	<i>10.84459</i>	<i>0.68925</i>	<i>31.11016</i>	<i>0.82898</i>	<i>30.99216</i>	<i>0.60879</i>
<i>12.33173</i>	<i>0.99981</i>	<i>12.33501</i>	<i>0.29032</i>	31.92197	0.99340	31.91777	0.18332
15.41686	0.99990	15.41680	0.01730	<i>32.34692</i>	<i>0.93750</i>	<i>32.38753</i>	<i>0.37163</i>
<i>15.95522</i>	<i>0.93615</i>	<i>16.02489</i>	<i>0.26457</i>	32.65153	0.99340	32.65182	0.10739
<i>16.03284</i>	<i>0.99941</i>	<i>16.04093</i>	<i>0.28087</i>				

TABLE 4. Computed eigenvalues  $\mu$  of  $\mathcal{L}_s$  in  $U(1, 33, 1, \delta^*)$  for the left bulb, paired with matched eigenvalues  $\lambda$  of  $\mathcal{L}$  and localization measures  $\delta(\psi, R)$  of their corresponding eigenvectors  $\phi$ . The 9 false indicators are highlighted in italics.

in Section 3, on a wide variety of problems, with a view toward providing guidance on how to set key parameters.

#### REFERENCES

- [1] G. Alessandrini. On Courant’s nodal domain theorem. *Forum Mathematicum*, 10(5):521–532, jan 1998.
- [2] R. Altmann, P. Henning, and D. Peterseim. Quantitative Anderson localization of Schrödinger eigenstates under disorder potentials. *Math. Models Methods Appl. Sci.*, 30(5):917–955, 2020.
- [3] R. Altmann and D. Peterseim. Localized computation of eigenstates of random Schrödinger operators. *SIAM J. Sci. Comput.*, 41(6):B1211–B1227, 2019.
- [4] D. N. Arnold, G. David, M. Filoche, D. Jerison, and S. Mayboroda. Computing spectra without solving eigenvalue problems. *SIAM J. Sci. Comput.*, 41(1):B69–B92, 2019.
- [5] D. N. Arnold, G. David, M. Filoche, D. Jerison, and S. Mayboroda. Localization of eigenfunctions via an effective potential. *Communications in Partial Differential Equations*, 44(11):1186–1216, 2019.
- [6] D. N. Arnold, G. David, D. Jerison, S. Mayboroda, and M. Filoche. Effective confining potential of quantum states in disordered media. *Phys. Rev. Lett.*, 116:056602, Feb 2016.
- [7] A. P. Austin and L. N. Trefethen. Computing eigenvalues of real symmetric matrices with rational filters in real arithmetic. *SIAM J. Sci. Comput.*, 37(3):A1365–A1387, 2015.
- [8] W.-J. Beyn. An integral method for solving nonlinear eigenvalue problems. *Linear Algebra Appl.*, 436(10):3839–3863, 2012.
- [9] W.-J. Beyn, C. Effenberger, and D. Kressner. Continuation of eigenvalues and invariant pairs for parameterized nonlinear eigenvalue problems. *Numer. Math.*, 119(3):489–516, 2011.
- [10] W.-J. Beyn, Y. Latushkin, and J. Rottmann-Matthes. Finding eigenvalues of holomorphic Fredholm operator pencils using boundary value problems and contour integrals. *Integral Equations Operator Theory*, 78(2):155–211, 2014.
- [11] N. Burq and M. Zworski. Bouncing ball modes and quantum chaos. *SIAM Rev.*, 47(1):43–49, 2005.
- [12] J. Canosa and R. G. D. Oliveira. A new method for the solution of the Schrödinger equation. *Journal of Computational Physics*, 5(2):188–207, apr 1970.
- [13] A. L. Delitsyn, B. T. Nguyen, and D. S. Grebenkov. Exponential decay of laplacian eigenfunctions in domains with branches of variable cross-sectional profiles. *The European Physical Journal B*, 85(11):17 (371), Nov. 2012.
- [14] E. Di Napoli, E. Polizzi, and Y. Saad. Efficient estimation of eigenvalue counts in an interval. *Numer. Linear Algebra Appl.*, 23(4):674–692, 2016.
- [15] M. Filoche and S. Mayboroda. Universal mechanism for Anderson and weak localization. *Proc. Natl. Acad. Sci. USA*, 109(37):14761–14766, 2012.
- [16] N. Garofalo and F.-H. Lin. Unique continuation for elliptic operators: A geometric-variational approach. *Communications on Pure and Applied Mathematics*, 40(3):347–366, may 1987.
- [17] J. Gopalakrishnan, L. Grubišić, and J. Owall. Spectral discretization errors in filtered subspace iteration. *Math. Comp.*, 89(321):203–228, 2020.
- [18] J. Gopalakrishnan, L. Grubišić, J. Owall, and B. Parker. Analysis of FEAST spectral approximations using the DPG discretization. *Comput. Methods Appl. Math.*, 19(2):251–266, 2019.

- [19] J. Gopalakrishnan and B. Q. Parker. Pythonic FEAST. Software hosted at <https://bitbucket.org/jayggg/pyeigfeast>.
- [20] D. S. Grebenkov and B.-T. Nguyen. Geometrical structure of Laplacian eigenfunctions. *SIAM Rev.*, 55(4):601–667, 2013.
- [21] S. Güttel, E. Polizzi, P. T. P. Tang, and G. Viaud. Zolotarev quadrature rules and load balancing for the FEAST eigensolver. *SIAM J. Sci. Comput.*, 37(4):A2100–A2122, 2015.
- [22] A. Hassell, L. Hillairet, and J. Marzuola. Eigenfunction concentration for polygonal billiards. *Comm. Partial Differential Equations*, 34(4-6):475–485, 2009.
- [23] L. Hormander. Uniqueness theorems for second order elliptic differential equations. *Communications in Partial Differential Equations*, 8(1):21–64, jan 1983.
- [24] A. Horning and A. Townsend. FEAST for differential eigenvalue problems. *SIAM J. Numer. Anal.*, 58(2):1239–1262, 2020.
- [25] R. Huang, A. A. Struthers, J. Sun, and R. Zhang. Recursive integral method for transmission eigenvalues. *J. Comput. Phys.*, 327:830–840, 2016.
- [26] R. Huang, J. Sun, and C. Yang. Recursive integral method with Cayley transformation. *Numer. Linear Algebra Appl.*, 25(6):e2199, 12, 2018.
- [27] T. Ikegami and T. Sakurai. Contour integral eigensolver for non-Hermitian systems: a Rayleigh-Ritz-type approach. *Taiwanese J. Math.*, 14(3A):825–837, 2010.
- [28] A. Imakura, L. Du, and T. Sakurai. A block Arnoldi-type contour integral spectral projection method for solving generalized eigenvalue problems. *Appl. Math. Lett.*, 32:22–27, 2014.
- [29] P. W. Jones and S. Steinerberger. Localization of Neumann eigenfunctions near irregular boundaries. *Nonlinearity*, 32(2):768–776, 2019.
- [30] T. Kato. *Perturbation theory for linear operators*. Classics in Mathematics. Springer-Verlag, Berlin, 1995. Reprint of the 1980 edition.
- [31] J. Kestyn, E. Polizzi, and P. T. P. Tang. FEAST eigensolver for non-Hermitian problems. *SIAM J. Sci. Comput.*, 38(5):S772–S799, 2016.
- [32] A. Kleefeld. A numerical method to compute interior transmission eigenvalues. *Inverse Problems*, 29(10):104012, 20, 2013.
- [33] J. Liu, J. Sun, and T. Turner. Spectral indicator method for a non-selfadjoint Steklov eigenvalue problem. *J. Sci. Comput.*, 79(3):1814–1831, 2019.
- [34] J. Lu and S. Steinerberger. Detecting localized eigenstates of linear operators. *Res. Math. Sci.*, 5(3):33, aug 2018.
- [35] J. Marklof and Z. Rudnick. Almost all eigenfunctions of a rational polygon are uniformly distributed. *J. Spectr. Theory*, 2(1):107–113, 2012.
- [36] M. Marletta. Neumann-Dirichlet maps and analysis of spectral pollution for non-self-adjoint elliptic PDEs with real essential spectrum. *IMA Journal of Numerical Analysis*, 30(4):917–939, aug 2009.
- [37] M. Marletta and R. Scheichl. Eigenvalues in spectral gaps of differential operators. *J. Spectr. Theory*, 2(3):293–320, 2012.
- [38] B.-T. Nguyen and D. S. Grebenkov. Localization of Laplacian eigenfunctions in circular, spherical, and elliptical domains. *SIAM J. Appl. Math.*, 73(2):780–803, 2013.
- [39] E. Polizzi. Density-matrix-based algorithm for solving eigenvalue problems. *Phys. Rev. B*, 79(11), MAR 2009.
- [40] T. Sakurai and H. Sugiura. A projection method for generalized eigenvalue problems using numerical integration. In *Proceedings of the 6th Japan-China Joint Seminar on Numerical Mathematics (Tsukuba, 2002)*, volume 159, pages 119–128, 2003.
- [41] T. Sakurai and H. Tadano. CIRR: a Rayleigh-Ritz type method with contour integral for generalized eigenvalue problems. *Hokkaido Math. J.*, 36(4):745–757, 2007.
- [42] J. Schöberl. Netgen/NGSolve. Software hosted at <https://ngsolve.org/>.
- [43] J. Schöberl. C++11 implementation of finite elements in NGSolve. ASC Report 30/2014, Vienna University of Technology, 2014.
- [44] S. Steinerberger. Localization of quantum states and landscape functions. *Proc. Amer. Math. Soc.*, 145(7):2895–2907, 2017.
- [45] P. T. P. Tang and E. Polizzi. FEAST as a subspace iteration eigensolver accelerated by approximate spectral projection. *SIAM J. Matrix Anal. Appl.*, 35(2):354–390, 2014.
- [46] M. Van Barel. Designing rational filter functions for solving eigenvalue problems by contour integration. *Linear Algebra Appl.*, 502:346–365, aug 2016.
- [47] M. Van Barel and P. Kravanja. Nonlinear eigenvalue problems and contour integrals. *J. Comput. Appl. Math.*, 292:526–540, 2016.
- [48] W. Xiao, B. Gong, J. Sun, and Z. Zhang. A new finite element approach for the Dirichlet eigenvalue problem. *Appl. Math. Lett.*, 105:106295, 5, 2020.
- [49] X. Ye, J. Xia, R. H. Chan, S. Cauley, and V. Balakrishnan. A fast contour-integral eigensolver for non-Hermitian matrices. *SIAM J. Matrix Anal. Appl.*, 38(4):1268–1297, 2017.
- [50] G. Yin. A contour-integral based method for counting the eigenvalues inside a region. *J. Sci. Comput.*, 78(3):1942–1961, 2019.
- [51] G. Yin. A harmonic FEAST algorithm for non-hermitian generalized eigenvalue problems. *Linear Algebra and its Applications*, 578:75 – 94, 2019.
- [52] S. Yokota and T. Sakurai. A projection method for nonlinear eigenvalue problems using contour integrals. *JSIAM Lett.*, 5:41–44, 2013.

JEFFREY S. OVALL, FARIBORZ MASEEH DEPARTMENT OF MATHEMATICS AND STATISTICS, PORTLAND STATE UNIVERSITY,  
PORTLAND, OR 97201  
*Email address: jovall@pdx.edu*

ROBYN REID, FARIBORZ MASEEH DEPARTMENT OF MATHEMATICS AND STATISTICS, PORTLAND STATE UNIVERSITY, PORTLAND,  
OR 97201  
*Email address: reid3@pdx.edu*